ON ENERGY SURFACES AND THE RESONANCE WEB

ANNA LITVAK-HINENZON AND VERED ROM-KEDAR

Abstract. A framework for understanding the global structure of near integrable n d.o.f. systems is proposed. The goal is to reach a similar situation to the near integrable 1.5 d.o.f. systems, where one is able in a glance of the integrable phase portrait, understand where instabilities are expected to arise under small perturbations. It is suggested that the main tool for understanding the system structure is an energy-momentum bifurcation diagram (EMBD) and generalized Fomenko graphs - the *branched surfaces*. It is demonstrated that for some systems this procedure is sufficient for achieving a full qualitative description of the near-integrable dynamics. In particular, the persistent appearance of instabilities associated with resonant lower dimensional tori are discussed. The relation between the EMBD and the presentation of the energy surfaces in the frequency space is established. Finally, it is proved that topological changes in the energy surfaces topology are associated with strong resonances of lower dimensional tori.

1. Introduction

The study of the structure of energy surfaces of integrable systems and the study of resonances and instabilities in near integrable systems developed into vast disparate research fields. The relation between the two received very little attention. Indeed, near regular level sets of the integrable Hamiltonian, the standard Arnold-resonance web structure appears and the relation between the two fields reduces to the study of Arnold conjecture regarding instabilities in phase space. Here, we demonstrate that near singular level sets of the integrable Hamiltonian much information regarding possible instabilities of the near integrable case may be deduced from the structure of the energy surface and its relations with resonance surfaces. We suggest that by adding some information to the traditional energy-momentum diagrams, which we name energy-momentum bifurcation diagrams (EMBD), one achieves a global qualitative understanding of the near-integrable dynamics. We relate the geometrical properties of the surfaces corresponding to lower dimensional tori in this diagram to both bifurcations in the energy surface topology and the appearance of lower dimensional resonant tori.

Recall that integrable systems are foliated almost everywhere by n-tori[1], which may be expressed locally as a product of n circles on which the dynamics reduces to simple rotations (the action-angle coordinates). A given compact regular level set (the set of phase space points with given values of the constants of motion) may be composed of several such tori. The energy surface is composed of all level sets with the same energy. These iso-energy level sets have different number of

Date: March 24, 2003.

1991 *Mathematics Subject Classification.* 70H08, 37J20.

Key words and phrases. Near integrable Hamiltonians.

[1]For simplicity we consider here only the case of compact level sets.

components iff there exists a singular level set on this energy surface which is not smoothly conjugate to a collection of n-tori. Such singularities may be expressed locally, using the Arnold-Liouville-Nekhoroshev coordinates, as fixed points (and their homoclinic loops) in s d.o.f. subsystem ($s \leq n$), called the normal system, and simple tori in the remaining $n - s$ d.o.f. (see exact statements in the formulation section below, and Lerman and Umanskii [30] for a complete treatment). The regular n tori correspond to the case $s = 0$. The larger the s the more cases and possibilities one has for the behavior in the normal directions. The larger the $n-s$, the more possibilities to transfer between the different cases, namely to encounter bifurcations. In this context, Lerman and Umanskii work [30] is mainly concerned with $n = s = 2$, whereas Fomenko and Oshemkov work [15, 4], is mainly concerned with $n = 2$, $s = 1$. Here, we consider $s = 1$ and $n \geq 2$, studying the implications of phase space bifurcations as a source for instabilities in the near-integrable systems.

Our main result, Theorem 2 (section 7.3), roughly states that *the existence of non-degenerate $n - 1$ dimensional torus of fixed points implies bifurcations in the topology of the energy surface*. Furthermore we prove that such a torus appears as an extrema of certain surfaces in the EMBD. In other words, this provides relation between energy surface topology, bifurcations in the EMBD and lower dimensional resonant tori.

Since the integrable system has n integrals of motion, a representation of the energy surfaces corresponds to indicating the range of allowed motion and its character in some n dimensional space (the innocent words "its character" hide a vast body of work dedicated to understanding the topology of the level sets which are represented as points in this reduced space as discussed below). Traditional spaces for such representation are the frequency domain [25], the space of constants of motion (e.g. [2, 30, 36, 17, 16]), the energy-momentum space and the momentum space (e.g. [2, 1, 6, 7, 43, 9, 30, 36]). Such presentations are all equivalent near regular level sets, where action-angle coordinates may be introduced. Furthermore, each of these representation is inherently non-unique as one may choose any non-singular vector function of the conserved quantities to serve as the new set of coordinates. We propose that a convenient representation appears in a specific combination of energy and momentum space. Convenient here means:

C1: The geometric presentation supplies a concise summary of all the dynamics and geometrical features of the integrable system for all energy levels.

C2: The geometric presentation provides clear criteria for the location of special regions in phase space which are expected to produce strong instabilities under a given form of a perturbation.

While many presentations in the n dimensional space satisfy the first criteria, it appears that the second one has not been explicitly addressed. Notice that the first criteria deals with the integrable part of the Hamiltonian only. On the other hand the second one depends on the nature of the applied perturbation, hence *the choice of the most convenient representation of the integrable system depends on the form of the perturbation*. These issues are explained more fully in section 3 where we propose a choice of convenient coordinates. Similar approach, in which the perturbation determines the appropriate integrable system is taken in the partial averaging procedure. Other related works, in which the geometry of the energy surfaces and their intersection with the resonance web are related to the perturbed

dynamics, are those on "resonance streaming", where it is argued that in 2 d.o.f. integrable systems a small angle between the intersecting resonance and energy curves (plotted in the frequency space) enhances the effect of added noise [31, 44].

The various representations in the n dimensional spaces of the constants of motion identify the regions of the allowed motion but do not, in general, supply information regarding the topology of the level sets. Indeed, the classification of all the possible topologies of the level sets of energy surfaces of integrable Hamiltonians is extremely challenging (see [2, 30, 36, 16, 1, 43]) and has been completed for the 2 d.o.f. case only [16, 30]. Lerman and Umanskii use the $n = 2$ integrals of motion near fixed points to obtain local and global information regarding the level sets of the integrable motion and to classify all possible generic homoclinic connections which are induced by the local behavior [27, 28, 29]. We use their formulation in our treatment of lower dimensional tori. Fomenko and co-workers suggested to use graphs to represent all topologically distinct tori which appear in the integrable dynamics [16, 17, 15, 39, 4]. Some of these ideas have been extended to classify integrable 3 d.o.f. dynamics such as the motion of rigid body [16, 9, 10]. Oshemkov, Fomenko and co-workers use the 2 d.o.f. constructions on given level sets of the third integral to analyze such systems [39, 16, 17]. Dullin *et al.* (see e.g. [9, 10, 47] and references therein) have shown that such approaches may be used to develop schemes for computing action-angle coordinates even when the topology of the energy surfaces is complicated and finding n topologically independent circles (n circles which are irreducible to each other) is an a priori complicated task. Here we investigate the structure of energy surfaces with very simple topological structure for which we are able to generalize Fomenko-Oshemkov graphs to branched surfaces.

The paper is ordered as follows; in section 2 we describe the type of the near-integrable Hamiltonians we study, with prototype examples of 3 d.o.f. systems which demonstrate the appearance of non-trivial energy surfaces. In section 3 we propose a convenient choice of momentum, and explain how the choice of suitable coordinates depends on the form of the perturbation. In section 4 we describe the structure of the energy surfaces and the resonance web in the frequency space and in the energy momentum space near normally elliptic lower-dimensional tori. The integrable structure in this a priori stable case is trivial and we add essentially no new insights to the known results. It is included here to build intuition for the next two sections. In section 5, we describe these structures near level sets corresponding to normally hyperbolic invariant $(n-1)$-tori. In section 6 we proceed to describe these structures near normally parabolic tori. In section 7 we formulate the notion of branched surfaces and topological bifurcations of the energy surfaces and prove our main theorems. We conclude with a discussion section.

2. Formulation

Consider a near integrable Hamiltonian $H_0(q,p) + \varepsilon H_1(q,p;\varepsilon), (q,p) \in M \subseteq \mathbb{R}^n \times \mathbb{R}^n$, where M is a $2n$-dimensional, smooth, symplectic manifold, $H_0 \in C^r(M)$, and H_1 is analytic in q, p and ε. H_0 represents the completely integrable part of the Hamiltonian, having n linearly independent integrals of the motion (the unperturbed system) and its structure is described below. On each energy level $H = h$, H_1, the Hamiltonian perturbation, is assumed to be *uniformly bounded* in the C^r topology. For any ε, a perturbed orbit with energy h resides on the energy

surface $H_0(\cdot) = h - \varepsilon H_1(\cdot;\varepsilon)$. Hence, the structure of the unperturbed energy surfaces and their resonance webs in an $O(\varepsilon)$-interval of energies near h supplies global information on the allowed range of motion of the perturbed orbits [34, 35].

The integrable n d.o.f. Hamiltonian, $H_0(q,p)$; $(q,p) \in M \subseteq \mathbb{R}^n \times \mathbb{R}^n$, has n independent integrals of motion: $H_0 = F_1, F_2, ..., F_n \in C^\infty(M)$, which are pair wise in involution: $\{F_i, F_j\} = 0$; $i,j = 1,...n$. Assume that $n \geq 3$ and that the Hamiltonian level sets, $M_g = \{(q,p) \in M, \quad F_i = g_i; \quad i = 1,...,n\}$, are closed and compact. By the Liouville-Arnold theorem (see [38] and [2, 24]), the connected compact components of the level sets M_g, on which all of the dF_i are (point wise) linearly independent, are diffeomorphic to n-tori and hence a transformation to action-angle coordinates ($H_0 = H_0(I)$) near such level sets is nonsingular. Consider a neighborhood of a possibly singular level set M_g; on each such connected and closed Hamiltonian level set there is some neighborhood D, in which the Hamiltonian $H_0(q,p)$ may be transformed to the form:

$$H_0(x,y,I), \qquad (x,y,\theta,I) \in U \subseteq \mathbb{R}^s \times \mathbb{R}^s \times \mathbb{T}^{n-s} \times \mathbb{R}^{n-s} \tag{2.1}$$

which does not depend on the angles of the tori, θ. The symplectic structure of the new integrable Hamiltonian (2.1) is $\sum_{j=1}^{s} dx_j \wedge dy_j + \sum_{i=1}^{n-s} d\theta_i \wedge dI_i$, where (θ, I) are the action-angle variables ($s = 0$ corresponds to the maximal dimensional tori - the n-tori discussed above). The motion on the $(n-s)$ dimensional family (parameterized by the actions I) of $(n-s)$-tori is described by the equations:

$$\dot{\theta}_i = \omega_i(x,y,I), \quad \dot{I}_i = 0.$$

The geometrical structure of the new Hamiltonian, $H_0(x,y,I)$, is such that for any fixed I an $(n-s)$-torus is attached to every point of the (x,y) plane (space, for $s > 1$). The (x,y) plane (space) is called the *normal plane* (*space*) [2, 40, 3] of the $(n-s)$-tori, and defines their stability type in the normal direction to the *family*[2] of tori. Invariant lower dimensional tori, of dimension $(n-l)$, generically exist for each $1 \leq l \leq n-1$; indeed, for any given s consider an m-resonant value of I. Then, for each such I, there exists an m dimensional family (corresponding to different initial angles) of $n-s-m$ dimensional tori. All these tori belong to the higher $n-s$ dimensional resonant torus, associated with I. The existence of such lower dimensional tori is restricted to the $n-s-m$ dimensional resonant surface of I values. A different type of lower dimensional invariant tori, which are of the main interest here, correspond to isolated fixed point(s) of the s-dimensional normal space. These appear on an $n-s$ dimensional manifold of I values, the singularity manifold (such a generalized fixed point corresponds to a manifold on which each dF_i for $i = 1,...,s$ is linearly dependent on $dI_1, ..., dI_{n-s}$). Locally, one may choose the (x,y,I) coordinate system so that for these tori:

$$\nabla_{(x,y)} H_0(x,y,I)\big|_{p_f} = 0, \qquad p_f = (x_f, y_f, I_f). \tag{2.2}$$

Hereafter, consider the case $s = 1$ only. The invariant $(n-1)$-tori have an $(n-1)$-dimensional vector of inner frequencies, $\dot{\theta} = \omega(p_f)$. The normal stability type of such families of $(n-1)$-tori is determined by the characteristic eigenvalues (respectively, Floquet multipliers for the corresponding Poincaré map) of the linearization

[2]Notice that a single torus belonging to this family has neutral stability in the actions directions. The normal stability referred too in the Hamiltonian context ignores these directions, see [5, 3] and references therein.

of the system about the tori; generically, these tori are either normally elliptic[3] or normally hyperbolic[4]. If the torus has one pair of zero characteristic eigenvalues in the direction of the normal (x, y) space, it is said to be *normally parabolic*. In addition, the *normal frequency*[5] [2, 40], Ω, of the $(n-1)$-tori is defined as the (non-negative) imaginary part of the purely imaginary characteristic eigenvalues[6].

Locally, in the (x, y, I) coordinate system, the normal stability of the invariant torus is determined by:

$$\det\left(\left.\frac{\partial^2 H_0}{\partial^2(x,y)}\right|_{p_f}\right) = -\lambda_{p_f}^2 \tag{2.3}$$

where p_f satisfies (2.2). Indeed, when λ_{p_f} is real and non-vanishing the corresponding family of tori is said to be normally hyperbolic, when it vanishes it is called normally parabolic and when it is pure imaginary it is normally elliptic. For more details on the above see [2, 5, 11, 12, 13, 14, 20, 21, 22, 23, 24, 40, 3] and references therein.

An example of a 3 d.o.f. integrable Hamiltonian which is in the form (2.1), possesses families of invariant 2-tori of all three normal stability types at $x = y = 0$ and satisfies all the stated above assumptions, is:

$$H_{bif}(x, y, I_1, I_2) = \frac{y^2}{2} - \frac{x^2}{2} I_1 + \frac{x^4}{4} + (\mu_1 + \frac{1}{2})\frac{I_1^2}{2} + \frac{I_2^2}{2} + \alpha_2 I_2 + \alpha_3 I_1 I_2 \tag{2.4}$$

where the α_i's and μ_1 are fixed parameters. We may compare it with a standard model of a priori stable systems with bounded energy surfaces having a family of normally elliptic 2-tori at $x = y = 0$:

$$\begin{aligned} H_{st}(x, y, I_1, I_2) &= \frac{y^2}{2} + \frac{x^2}{2} + \frac{x^4}{4} + \alpha_1 I_1 + \alpha_2 I_2 + \frac{I_1^2}{2} + \frac{I_2^2}{2} \\ &= \sum_{i=0}^{2} \left(\alpha_i I_i + \frac{I_i^2}{2}\right), \qquad \alpha_0 = 1 \end{aligned} \tag{2.5}$$

and to the corresponding a priori unstable system:

$$H_{ust}(x, y, I_1, I_2) = \frac{y^2}{2} - \frac{x^2}{2} + \frac{x^4}{4} + \alpha_1 I_1 + \alpha_2 I_2 + \frac{I_1^2}{2} + \frac{I_2^2}{2} \tag{2.6}$$

which has a family of normally hyperbolic 2-tori at $x = y = 0$.

3. The dependence of the presentation on the form of the perturbation.

To proceed, we first recall the trivial geometry of the resonance surfaces in the frequency space. Consider a phase space domain where all level sets of the integrable Hamiltonian are regular and compact, so that the transformation to action-angle coordinates $(\theta, I) \in \mathbb{T}^n \times \mathbb{R}^n$ in this domain is regular and the frequency vector $\omega(I)$

[3] If all the characteristic eigenvalues of an invariant lower dimensional torus (with respect to its normal (x, y) space), are purely imaginary (and do not vanish), it is said to be *normally elliptic*.

[4] If all the characteristic eigenvalues of an invariant lower dimensional torus (with respect to its normal (x, y) space) have a nonzero real part, it is said to be *normally hyperbolic*.

[5] In some references, these are called characteristic frequencies.

[6] In some references, e.g. [5], the normal frequencies are defined as the positive imaginary parts of all the characteristic eigenvalues.

is well defined. In such domains the dynamics is equivalent to that of n non-linear oscillators with amplitude vector I. The resonance surfaces, which are given by the frequencies satisfying $\langle k, \omega \rangle = 0$, are co-dimension one hyper-planes, passing through the origin of the frequency space. The energy surfaces themselves may have non-trivial structure in the frequency space - both topologically and geometrically. As we will demonstrate below it is therefore beneficial to plot them in additional space - the energy-momentum space. However, before embarking into detailed analysis of these surfaces in these different coordinates systems an important natural question arises - what is the significance of the different representations if they are coordinate dependent? In particular, it is clear that a general symplectic transformation from the (θ, I) coordinates to the (φ, J) coordinates changes some geometrical properties of the energy surface. Furthermore, transformations of the form $(\theta, I) \to (\varphi = \theta - \varpi t, I)$, which correspond to moving relative to particular tori with frequency vectors $\omega = \varpi$, for which $H_{new}(J) = H_0(J) - \varpi J$ where $\dot{\theta} = \frac{\partial H_0(I)}{\partial I}$, may change the topology of the energy surfaces, the structure of their singularity manifolds and the nature of their intersections with the resonance hypersurfaces. In fact, we may even take $\varpi = \varpi(I)$, with $H_{new}(J) = H_0(J) - \overline{H}(J)$ where $\varpi(I) = \frac{\partial \overline{H}(I)}{\partial I}$, which demonstrates that we may deform the energy surface in almost arbitrary way. Hence, it appears that indeed finding the "correct" representation is ill-defined in the context of the integrable system. *We propose that the form of the perturbation resolves these issues.*

Consider first the issue of moving frames. The transformation $(\theta, I) \to (\varphi = \theta - \varpi(I)t, I)$, produces in general time-dependent Hamiltonians, hence, the coefficients $\varpi(I)$ may be determined by requiring that the transformed Hamiltonian is autonomous (if such a transformation is possible). Notice that if we start with an autonomous near-integrable system $H = H_0(q,p) + \varepsilon H_1(q,p) = H_0(I) + \varepsilon H_1(\theta, I)$, we immediately obtain that generally $\varpi(I)$ must vanish identically to preserve the autonomous character of the problem. This trivial statement implies, in particular, that given an a priori stable near integrable system of the form (2.5), for generic vector α, it may not be transformed to the system with $\alpha = 0$ without introducing time-dependent perturbations.

The second issue which arises is the choice of the action variables, which implicitly determines which resonances are considered strong. This issue is well understood in the context of averaging [2]; the form of the anticipated *perturbation* determines which of the resonant surfaces will produce the strongest response; consider the near integrable system, expressed near a singular level set in some local Arnold-Liouville-Nekhoroshev coordinates:

$$H(q,p) = H_0(x,y,I) + \varepsilon H_1(x,y,\theta,I). \tag{3.1}$$

Consider the Fourier series of H_1:

$$H_1(q,p) = H_1(x,y,\theta,I) = \sum_{|k|=|k_1|+\cdots+|k_n| \geq r_0} h_k(x,y,I) \exp(\mathrm{i}\,\langle k, \theta \rangle).$$

Then, provided h_k are monotonically decreasing (we assume H_1 is analytic, so h_k decays exponentially for large $|k|$) the strongest resonances are given by the frequencies satisfying $\langle k, \omega \rangle = 0$ for k values which are included in the sum ($h_k \neq 0$ near the singular level set) and satisfy $|k| \approx r_0$, see [2] for exact definition and discussion. In particular, by a change of the action angle coordinates $(\theta, I) \to (\phi, J)$

one may arrange so that the first n terms in the above sum have $k^j = r_j e_n^j = (0, ..., r_j, ...0)$ for $j = 1, \ldots, n$ (where r_j is in the j^{th} place, and are monotonically increasing with j). Then, the strongest resonances occur along the action variables directions.

Summarizing the above observations, we propose:

Definition 1. *The local Arnold-Liouville-Nekhoroshev coordinates (x, y, θ, I) of the integrable part of a near-integrable system are called suitable if:*

- *The perturbed system is autonomous.*
- *The strongest $n - s$ resonant terms are aligned, in decreasing order, along the $n - s$ actions. More precisely, let*

$$H_1(q,p) = H_1(x,y,\theta,I) = \sum_j h_{k^j}(x,y,I)\exp(\mathrm{i}\left\langle k^j, \theta\right\rangle), \quad j \in \mathbb{N} \tag{3.2}$$

with $\left|k^j\right|$ monotonically increasing with j and $\|h_{k^j}\|$ monotonically decreasing with j for equal $\left|k^j\right|$ values. Then, $k^j || e_{n-s}^j$ (i.e. k^j is parallel to e_{n-s}^j), for $j = 1, .., n - s$, where e_{n-s}^j is the $n - s$ dimensional unit vector with 1 at the j^{th} entry.

Lemma 1. *If (x, y, θ, I) and (q, p, φ, J) are two suitable coordinates for the system (3.1) then $I = J$ and $\varphi = \theta + f(I)$.*

Proof. First, notice that the requirement that I, θ and J, φ are action-angle coordinates implies that a general symplectic transformation between these two coordinate systems must satisfy:

$$J = g(x,y,I), \qquad \varphi = \left(\frac{\partial g}{\partial I}\right)^{-1}\theta + f(I)$$

for some analytic functions g, f. Expressing the perturbed part of the Hamiltonian in the (x, y, θ, I) coordinates and using the above transformation in (3.2), we obtain

$$H_1(q,p,\varphi,J) = \sum_j \widetilde{h_{k^j}}(q,p,J)\exp(\mathrm{i}\left\langle k^j, \frac{\partial g}{\partial I}\varphi\right\rangle)$$

with $k^j || e_{n-s}^j$ for $j = 1, .., n - s$. Therefore, insisting that q, p, φ, J are suitable implies that for all φ:

$$\left\langle e_{n-s}^j, \frac{\partial g}{\partial I}\varphi\right\rangle = \left\langle e_{n-s}^j, \varphi\right\rangle \quad \text{for} \quad j = 1, .., n-s$$

hence that $\frac{\partial g}{\partial I} = Id$. Since g is analytic and $\frac{\partial g}{\partial I} = Id$ in an open neighborhood of the singular level set, it follows that $g(x, y, I) = I$. □

Conversely, one may take the usual convention by which, given an integrable Hamiltonian in a given coordinate system, the analysis determines which form of the perturbation will cause the largest instability in the vicinity of a given resonance junction. In particular, by the appropriate change of coordinates of the integrable system, one obtains that the *strongest* resonances possible are realized when $k = e_n^j = (0, 0, ..., 0, 1, 0, ..., 0)$. With this view the notion of strongest resonances is inherently coordinate dependent.

In our presentation of the energy surfaces in the energy-momentum plots we relate changes in the energy surface singular structures to strong resonances of

lower dimensional tori. To make such statements well defined, we insist that the coordinates we use are locally suitable coordinates.

4. A priori stable systems

To obtain a good understanding of our proposed presentation of the energy-momentum bifurcation diagram (EMBD) we begin with the simplest and most familiar model of a priori stable systems near lower dimensional torus. Let us examine the presentation of the regular part of the energy surface first in the frequency space, and then in the energy-momentum space.

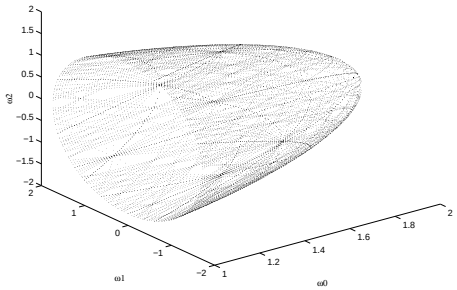

FIGURE 1. A resonance web on a cap of an energy surface of an a priori stable system (eq. (4.1) with $h = 0.5$).

4.1. **Energy surfaces in the frequency space (S).** For the standard Hamiltonian H_{st} (see equation (2.5)) the transformation from momentum to frequency variables is a shift ($\omega(I) = \alpha + I, \quad \alpha = (1, \alpha_1, \alpha_2)$), and is regular everywhere, so we can write:

$$H_{st}(I) = H_{st}(\omega) = \frac{1}{2}\|\omega(I)\|^2 - \frac{1}{2}\|\alpha\|^2 \tag{4.1}$$

and we obtain the standard result that in the definite case the energy surfaces appear in the frequency space as spheres centered at $\omega = 0$. The natural oscillations near the elliptic fixed point $x = y = 0$ (where the transformation from the (x, y) coordinates to the action-angle coordinates is singular) corresponds to the circle $\omega_0 = \alpha_0 = 1$, and in this representation appears as a regular level set of the energy surface. Here it is natural to insist on positive I_0 value, leading to energy surfaces in the form of "caps" with boundaries: $\omega^h = \{\omega | \ \|\omega\|^2 = 2h + \|\alpha\|^2, \omega_0 \geq \alpha_0 = 1\}$. The boundary $\omega_0 = \alpha_0$ corresponds to the family of lower dimensional tori $x = y = 0$ on the given energy surface, see figure 1. In the figure we also show the dense intersection of the resonance surfaces, given by planes passing through the origin, with this cap (see [2, 22, 31] and references therein). The planes $\omega_i \equiv 0$, $i = 0, 1, 2$ correspond to the strongest resonances. Notice that the only energy surface which includes the origin is a sphere with diminishing radius, and such an energy surface is disallowed for systems of the form (4.1).

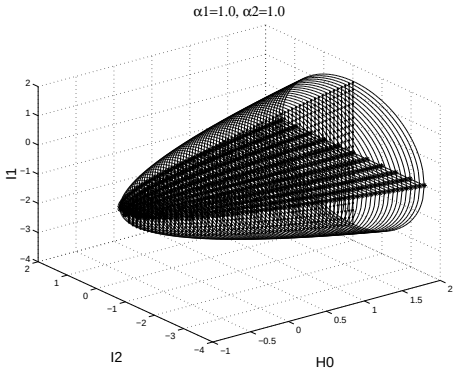

FIGURE 2. Energy-momentum bifurcation diagram of an a priori stable system

4.2. **Energy surfaces in the Energy-Momentum space (S).** Alternatively, in figure 2, we construct the EMBD of the system (2.5) by presenting the energy surfaces in the space (H_0, I_1, I_2) where $H_{st}(x, y, I) = H_0$. For any given energy $H_0 = h$, the allowed region of motion is bounded by the family of normally elliptic 2-tori $(x, y, I) = (0, 0, I(h))$. The corresponding singularity surface in the EMBD is given by the paraboloid:

$$p^0_{ell}(h, I_1, I_2) = \left\{ (h, I_1, I_2) | \quad H_{st}(0, 0, I) = \frac{1}{2} \sum_{i=1}^{2} \left((\alpha_i + I_i)^2 - \alpha_i^2 \right) = h, \ h \geq h_{ell} = 0 \right\},$$

namely, for a given h, (I_1, I_2) belong to a circle of radius $\sqrt{2h + \alpha_1^2 + \alpha_2^2}$ which is centered at $(-\alpha_1, -\alpha_2)$.The singularity manifolds corresponding to *normally elliptic* invariant tori are denoted by a collection of *solid* curves in the EMBD as demonstrated in figure 2. To see that motion is allowed only for I values which are interior to this paraboloid notice that from (2.5):

$$0 \leq \frac{y^2}{2} + \frac{x^2}{2} + \frac{x^4}{4} = h - \frac{1}{2} \sum (I_i + \alpha_i)^2 + \frac{\alpha_1^2 + \alpha_2^2}{2}.$$

The energy surfaces which appear as caps in the frequency space are "flattened" here to discs in the energy-momentum space. An example of an energy surface in the (I_2, I_1) plane, corresponding to the 2D slice of figure 2 at $H_0 = 1$, is presented in figure 3A. The thin vertical lines in the 2D sections of the EMBD indicate the region of allowed motion. In 3B we present a 2D slice in the (H_0, I_1) plane at $I_2 = 0$, on which we schematically indicate the corresponding Fomenko graph by a thick black line. The Fomenko graph for any positive h and an interior I_2 value is simply a segment: each interior point on this segment corresponds to a single 3-torus, and each of the end points corresponds to a normally elliptic 2-torus ("atom A" in [17]). For such a fixed I_2 value the energy surface appears as a 2-sphere in the (x, y, I_1) space. The poles of this sphere are normally elliptic 2 dimensional tori, and they correspond to the boundaries of this component of the energy surface. Equivalently, we may think of a natural generalization of the Fomenko graphs to branched surfaces, and in this trivial case the branched surface is simply a single

disk, as shown in figure 9A: an interior point to the disc corresponds to a 3-torus, and a point on the disc boundary corresponds to a 2-torus.

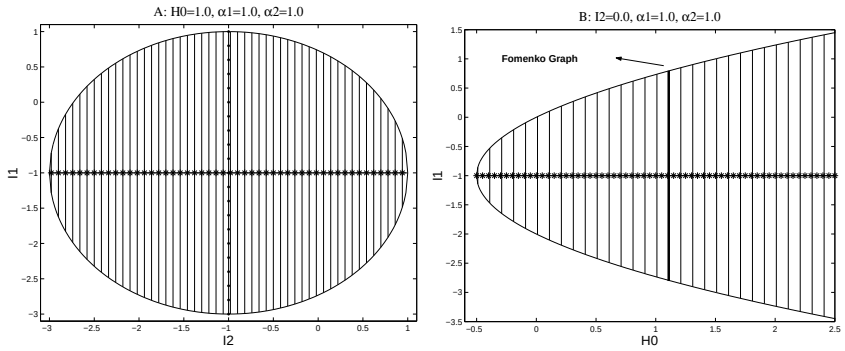

FIGURE 3. 2D slices of an energy-momentum bifurcation diagram of an a priori stable system: A - one energy surface, B - range of energy values for a fixed value of I_2 and a schematic Fomenko graph.

The *strong resonances* $\omega_i = 0, i = 1, 2$, correspond here to the hyperplanes $I_i = -\alpha_i$. Their intersections with the singularity manifold p^0_{ell} satisfies:

$$\dot{\theta}_i = \left.\frac{\partial H}{\partial I_i}\right|_{x=y=0, I_i=-\alpha_i} = \left.\frac{dH(p^0_{ell})}{dI_i}\right|_{x=y=0, I_i=-\alpha_i} = 0.$$

Namely, it *corresponds to a fold in the singularity manifold* p^0_{ell}. Here the relation between total derivatives w.r.t. I_i along p^0_{ell} and the corresponding partial derivatives of H is trivial. We notice that it is satisfied even when the location of the singularity manifold depends on I_i since $\nabla_{x,y} H$ vanishes on the singularity surfaces. This latter property is coordinate independent as long as the coordinates are suitable. It follows that the families of lower dimensional tori $\{(x, y, I) = (0, 0, -\alpha_1, I_2), H_{st}(0, 0, I) = h, I_2 \in \mathbb{R}\}$, $\{(x, y, I) = (0, 0, I_1, -\alpha_2), H_{st}(0, 0, I) = h, I_1 \in \mathbb{R}\}$ are strongly resonant. They intersect at the minimal possible energy where $(I_1, I_2) = (-\alpha_1, -\alpha_2)$, corresponding to a two-torus of fixed points. In figures 2 and 3 we indicate these strongest resonances by starred lines (for $\dot{\theta}_1 = 0$) and dotted lines (for $\dot{\theta}_2 = 0$).

4.3. **Qualitative behavior of the near-integrable system (S).** The motion in the near-integrable system $H(\theta, I) = H_{st}(I) + \varepsilon H_1(\theta, I)$ is restricted to the energy level $H = h$. Since $H_1(\theta, I)$ is assumed to be bounded in the C^r topology, we obtain that the unperturbed energy surfaces with $H_{st}(I) = h^*$, $|h^* - h| < C\varepsilon$ supply a-priori bound to the motion. For energy surfaces of large extent, such an a-priori bound is irrelevant due to Nekhoroshev type theorems and the Arnold conjecture. Hence, in this case the only new information obtained from the EMBD is regarding the appearance of strong lower-dimensional resonant tori (and even this information can be extracted from the frequency plot). Near the doubly resonant normally elliptic lower dimensional torus, where $(x, y, I) = (0, 0, -\alpha_1, -\alpha_2)$, one may expect small perturbations to produce large instabilities. Our trivial observation regarding

the extent of the energy surface immediately shows that the extent of the instability cannot be larger than $O(\sqrt{\varepsilon})$, the extent in the I space of the energy surfaces with $H_{st}(I) = h^*$, $|h^* - h| < C\varepsilon$. We may except that the behavior near the doubly-resonant torus will be dramatically different if the dependence on the actions is linear or indefinite:

$$H_{st-unbounded}(x, y, I_1, I_2) = \frac{y^2}{2} + \frac{x^2}{2} + \frac{x^4}{4} + \alpha_1 I_1 + \alpha_2 I_2 - \frac{I_1^2}{2} + \frac{I_2^2}{2}$$

namely, the energy surfaces are unbounded, and, in particular, the energy surface passing through the elliptic double resonant fixed point is unbounded. Such considerations are the trivial analogs to the non-linear stability theorems of Arnold-Marsden and have been studied and discussed in the context of normal forms near elliptic fixed points ([2],[36]).

5. A-priori unstable systems

The phase space structure of the standard Hamiltonian H_{ust} (equation (2.6)):

$$H_{ust}(x, y, I_1, I_2) = \frac{y^2}{2} - \frac{x^2}{2} + \frac{x^4}{4} + \frac{1}{2}\sum_{i=1}^{2}\left((\alpha_i + I_i)^2 - \alpha_i^2\right) \tag{5.1}$$

$$= H_{xy}(x, y) + H_I(I) \tag{5.2}$$

is given by the product of a figure eight motion in the xy plane and a family of 2-tori in the (θ, I) space. The precise structure of each energy surface, which demonstrates how a given energy may divide between the three modes (degrees of freedom) requires a bit more attention. Since there are no global action-angle coordinates in the (x, y) plane, it is instructive to start with the presentation of the energy surfaces in the energy-momentum space and then discuss the presentation in the frequency space.

5.1. **Energy surfaces in the Energy-Momentum space (U).** To construct the EMBD we find the singularity manifolds of the Hamiltonian (5.1). These manifolds correspond to fixed points of $H_{xy}(x, y)$. The normally elliptic singularity surfaces, corresponding to $\{x = \pm 1, y = 0\}$, are given by the identical[7] paraboloids:

$$p_{ell}^{\pm}(h, I_1, I_2) = \left\{(h, I_1, I_2) | \quad \frac{1}{2}\sum_{i=1}^{2}\left((\alpha_i + I_i)^2 - \alpha_i^2\right) = h + \frac{1}{4},\ h \geq h_{ell}\right\},$$

where

$$h_{ell} = -\frac{1}{4} - \frac{1}{2}\sum_{i=1}^{2}\alpha_i^2.$$

The normally hyperbolic singularity surface corresponding to $x = y = 0$ and its separatrices is given by the paraboloid

$$p_{hyp}^{0}(h, I_1, I_2) = \left\{(h, I_1, I_2) | \quad \frac{1}{2}\sum_{i=1}^{2}\left((\alpha_i + I_i)^2 - \alpha_i^2\right) = h,\ h \geq h_{hyp}\right\},$$

where

$$h_{hyp} = -\frac{1}{2}\sum_{i=1}^{2}\alpha_i^2.$$

[7]Adding an asymmetric term like ηx to H_{ust} lifts this degeneracy.

In figure 4 an EMBD of system (5.1) is presented as two nested paraboloids. The singularity manifolds are drawn according to the normal stability of the lower dimensional invariant tori they represent - the normally elliptic singularity manifolds ($p^{\pm}_{ell}(h, I_1, I_2)$) are drawn as a collection of solid curves whereas the *normally hyperbolic* singularity manifold ($p^{0}_{hyp}(h, I_1, I_2)$) is drawn as a collection of black *dashed* curves. Thus we follow the traditional notation in bifurcation diagrams.

Given an energy surface $H_{ust}(x, y, I_1, I_2) = H_0 = h$ with $h_{ell} \leq h < h_{hyp}$, the 3D and 2D EMBD look locally similar to those of the a priori stable system, presented in figures 2 and 3: for each fixed energy value in this range the energy surface is a disk in the (I_2, I_1) plane. However, each point interior to this disk corresponds to *two* sets of 3-tori, one in each well of the potential of $H_{xy}(x, y)$. Points on the boundary of the disk correspond to the *two* normally elliptic 2-tori, $\{x = \pm 1, y = 0, H_{ust}(\pm 1, 0, I_1, I_2) = h\}$. Hence, the Fomenko graph for any 1D section of each such disk is given by two disconnected segments, as shown in figure 5B. Equivalently, the generalized branched surfaces for this range of energies is the union of two disconnected discs (see figure 9B). Each point belonging to the interior of the branched surfaces represents, as before, a single 3−torus, and every point on the solid boundary of the discs represents, as before, a single, normally elliptic 2−torus. The multiplicity in the number of components of the level set corresponding to a given (h, I_1, I_2) is expressed by the multiplicity in the number of components of the branched surfaces for these values of (h, I_1, I_2). A precise construction of the branched surfaces is suggested in section 7.2.

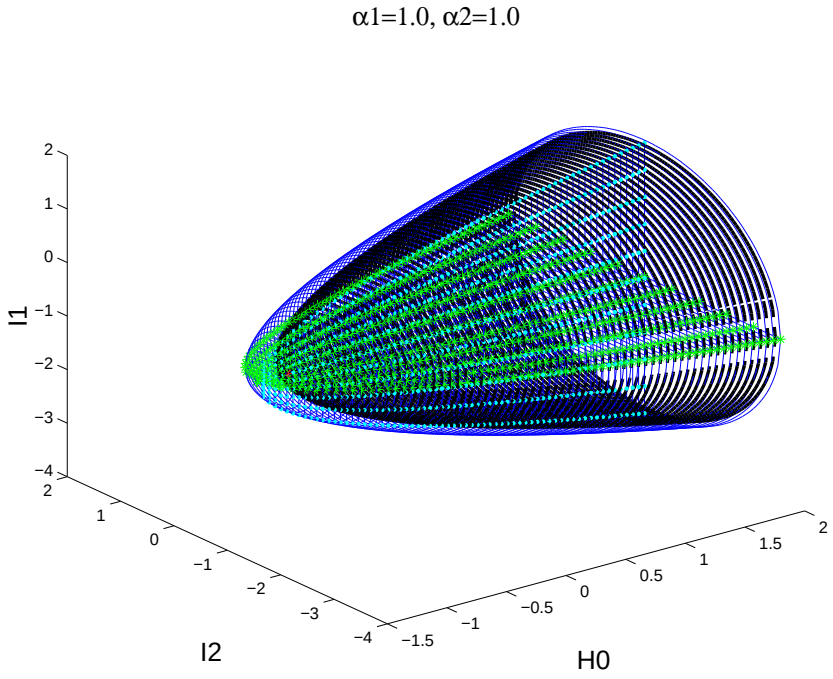

FIGURE 4. Energy-momentum bifurcation diagram of an a priori unstable system.

For $h \geq h_{hyp}$ the energy surfaces include the singular level set of the separatrices, which divides the energy surface to two topologically different regimes, see figure 5A. A point (h, I_1, I_2) inside the disk enclosed by $p^0_{hyp}(h, I_1, I_2)$ (the dashed circle in 5A) corresponds to a single 3-torus. Trajectories belonging to this torus encircle both wells in the xy plane. A point inside the ring bounded between $p^0_{hyp}(h, I_1, I_2)$ and $p^{\pm}_{ell}(h, I_1, I_2)$ corresponds to *two* sets of 3-tori - trajectories belonging to one of these tori oscillate in one of the wells in the xy plane. The Fomenko graph for this case is shown schematically on the cross-section in figure 5B (in thick black). The generalized branched surfaces here are two rings which are glued together in a central disk (figure 9C). Each regular point of the branched surface corresponds to a single 3−torus, each point belonging to the dashed circle corresponds to a normally hyperbolic 2−torus and its separatrices, and each point belonging to the solid (outer) boundaries of the rings corresponds to a single normally elliptic 2−torus.

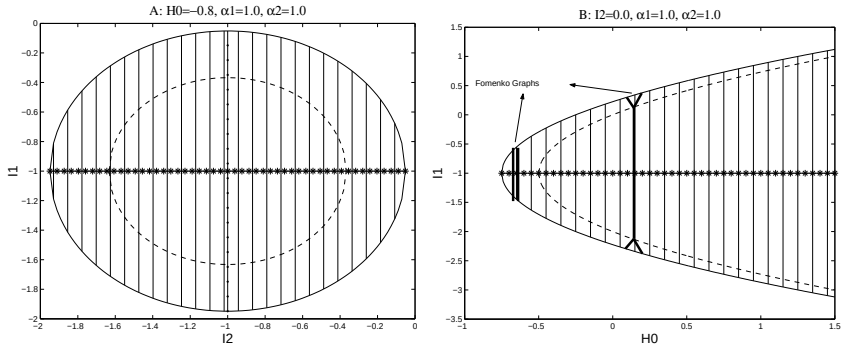

FIGURE 5. 2D slices of an energy-momentum bifurcation diagram of an a priori unstable system with $h > h_{hyp}$: A - one energy surface, B - range of energy values for a fixed value of I_2 and a schematic Fomenko graph.

Intersections of the singularity manifolds with the hypersurfaces of strongest resonances correspond to folds of these singularity manifolds in the EMBD (see figures 4 and 5). This is the essence of Theorem 1 (see section 7.1). For example, the paraboloids $p^0_{hyp}(h, I_1, I_2)$ and $p^{\pm}_{ell}(h, I_1, I_2)$ fold as they cross the surface $I_1 = -\alpha_1$ (and similarly at $I_2 = -\alpha_2$) and indeed $\dot{\theta}_i\Big|_{p_f} = \alpha_i + I_i$. Thus, the families of 2-tori, $p^{\pm}_{ell}(h, -\alpha_1, I_2)$, $p^{\pm}_{ell}(h, I_1, -\alpha_2)$, $p^0_{hyp}(h, -\alpha_1, I_2)$ and $p^0_{hyp}(h, I_1, -\alpha_2)$, are all resonant and the 2-tori $p^{\pm}_{ell}(h_{ell}, -\alpha_1, -\alpha_2)$ and $p^0_{hyp}(h_{hyp}, -\alpha_1, -\alpha_2)$ are doubly resonant - these are 2-tori of fixed points. In figure 4 the strong resonance in the I_1 direction ($\dot{\theta}_1 = 0$) is denoted by a surface of green starred lines and the strong resonance in the I_2 direction ($\dot{\theta}_2 = 0$) by a surface of cyan dotted lines; the *double fold* corresponding to a 2-resonant hyperbolic 2-torus (a hyperbolic torus of fixed points) is denoted by a red star.

Observe that the topology of the family of equi-energy normally hyperbolic lower dimensional tori ($p^0_{hyp}(h, \cdot)$, with fixed h) changes exactly at this double fold point, $p^0_{hyp}(h_{hyp}, -\alpha_1, -\alpha_2)$, where a 2-torus of fixed points resides; for $h < h_{hyp}$ the

singularity surface $p^0_{hyp}(h,\cdot)$ does not exist and the energy surfaces have two disconnected components (figure 9B) whereas for $h > h_{hyp}$ the singularity surface $p^0_{hyp}(h,\cdot)$ is a circle and the two components of the energy surface connect on this circle (figure 9C). This is the essence of Theorem 2 (see section 7.1). Similarly, for the natural n d.o.f. generalization of H_{ust}:

$$H^n_{ust}(x,y,I_1,...,I_{n-1}) = \frac{y^2}{2} - \frac{x^2}{2} + \frac{x^4}{4} + \frac{1}{2}\sum_{i=1}^{n-1}\left((\alpha_i+I_i)^2 - \alpha_i^2\right) \tag{5.3}$$

$$= H_{xy}(x,y) + H^n_I(I) \tag{5.4}$$

$p^0_{hyp}(h,\cdot)$ changes from non-existence for $h < h_{hyp}$ to an $n-2$ sphere for $h > h_{hyp}$. In particular, for $n=2$, there are either none or two non-resonant hyperbolic circles on each energy surface. If the dependence on the I variables is indefinite then one may have other topological changes in $p^0_{hyp}(h,\cdot)$ occurring at the $(n-1)$-resonant $(n-1)$-torus; either the genus of $p^0_{hyp}(h,\cdot)$ changes or two components of $p^0_{hyp}(h,\cdot)$ coalesce/separate. Notice that the flow along the lower dimensional $(n-1)$-torus reverses its direction as a strong resonance surface is crossed (namely, $\dot{\theta}_i\Big|_{p_f}$ changes its sign there). This property holds for the general case of non-separable systems as well (see [42, 35, 34]).

5.2. **Energy surfaces in the frequency space (U).** For small energy levels, $h_{ell} \le h < h_{hyp}$, we have seen that the disk $H_{ust}(x,y,I_1,I_2) = h$ in the (I_2,I_1) plane (see figures 5B and 9B) corresponds to two separate smooth compact components of the energy surface. In the frequency space these appear as a cap of hyperbola, centered at the origin. Indeed, the natural frequency in the xy plane at the elliptic points is $\omega_0(h,I_1,I_2)|_{p^{\pm}_{ell}(h,I_1,I_2)} = \sqrt{2}$, the direction of rotation is preserved for all orbits (so $\omega_0(h,I_1,I_2) \ge 0$) and the frequency monotonically decays as the action of the periodic orbits grows. Denoting by $\omega_{0\,\min}(h) > 0$ the frequency of the two symmetric periodic orbits in the xy plane satisfying $H_{xy}(x,y) = h$, it follows that for this range of energies

$$\omega_{0\,\min}(h) \le \omega_0(h,I_1,I_2) \le \sqrt{2}\ . \tag{5.5}$$

In figure 6 an example of such a cap shaped energy surface of system (5.1) in the frequency space is shown.

For $h \ge h_{hyp}$ the behavior near the separatrices needs to be presented. Since the frequency in the xy plane is well defined for all orbits except the separatrices, and since $\omega_0(x,y) \to 0$ as the separatrix is approached, defining $\omega_0(0,0) = 0$ makes $\omega_0(x,y)$ a continuous (non-differentiable) function of the xy energy level (this observation is used extensively in the Frequency map plots, see [26]). Hence, for $H_0 = h \ge h_{hyp}$, an energy surfaces in the frequency space has an annular cap component which meets at the (singular) circle $\omega_0 = 0$ a central cap, see figure 7. The annular cap corresponds to the two sets of tori for which the motion is restricted to one of the wells in the xy plane whereas the central cap corresponds to a single family of 3-tori for which the motion in the xy plane surrounds both wells of the potential. Recall that strong resonances are created when the energy surface intersects one of the $\omega_i = 0$ planes. However, here, the surface approaches

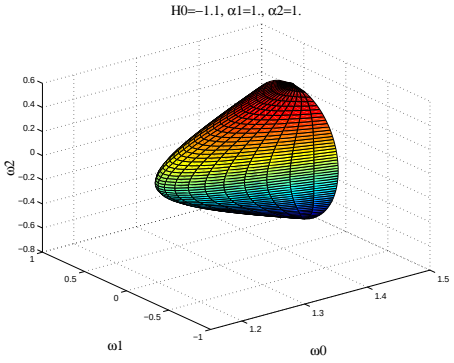

FIGURE 6. Energy surface of an a priori unstable system in the frequency space, for $h_{ell} < H_0 < h_{hyp}$

the plane $\omega_0 = 0$ singularly, and the normally hyperbolic torus is not resonant in the θ_0 direction.

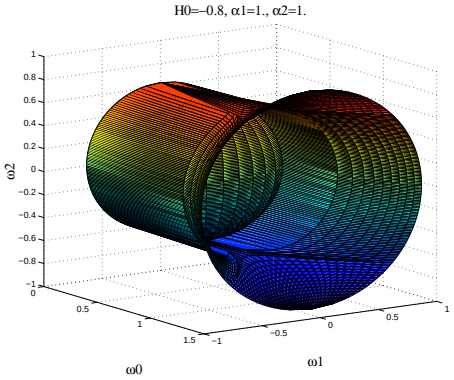

FIGURE 7. Energy surface of an a priori unstable system in the frequency space, for $H_0 > h_{hyp}$

5.3. **Qualitative behavior of the near-integrable system (U).** Using the plots of the EMBD we may read off all possible sources of instabilities for near integrable n d.o.f. systems with unperturbed Hamiltonian of the form (5.3). Here we need to combine several effects:

- Instabilities associated with the regular resonance web. Such instabilities may appear near any point in the EMBD.
- Instabilities associated with splitting of the separatrices (as in one and a half d.o.f. systems). Such instabilities may appear for any $h > h_{hyp}$ in an ε neighborhood of the surface $p^0_{hyp}(h, \cdot)$.
- Instabilities associated with the existence of families of separatrices on the same energy surface (as in Arnold's conjecture for the existence of whiskered transition chain). For $n \geq 3$, these appear for any $h > h_{hyp}$ near the surface $p^0_{hyp}(h, \cdot)$.

- Instabilities associated with strongly resonant normally hyperbolic tori. For $k < n-1$, the $k-$resonant normally hyperbolic tori appear for all $h > h_{hyp}$, and their effect must be included in the above mentioned transition chain.
- Instabilities associated with bifurcations in the structure of the singularity manifolds as the energy varies. These appear near the critical energy surface $h = h_{hyp}$ near the singularity surface $p^0_{hyp}(h, \cdot)$. There, $p^0_{hyp}(\cdot)$ has an $n-1$ fold point and the normally hyperbolic torus $p^0_{hyp}(h_{hyp}, \cdot)$ is a torus of fixed points.

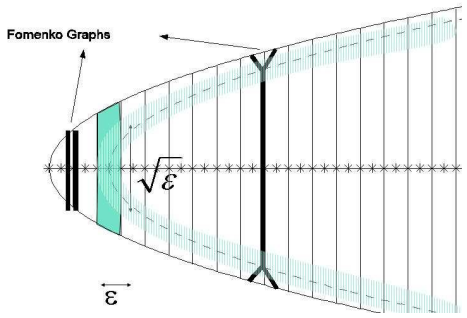

FIGURE 8. 2d slice of the EMBD of the perturbed motion. Shaded Strip - region of allowed motion for perturbed orbits near hyperbolic resonance. Dashed region - homoclinic chaos region.

While the detailed analysis of each of the above items is not yet well understood, we propose that the inclusion of rough lower bounds on the instability associated with each of the above phenomena supplies nontrivial information on the system. In figure 8 we plot on a 2D slice of the EMBD an $O(\varepsilon)$ band around the separatrix level sets (the light shaded region), and indicate an $O(\varepsilon)$ slab of energies to which the perturbed motion is restricted near a hyperbolic resonance (the dark shaded strip). The geometry near the hyperbolic resonant tori immediately presents itself as a source for larger instabilities than the non-resonant terms. A detailed analysis of this case for $n = 2$ has been developed, see [22] and references therein. Here we see that in the 3-d.o.f. context the hyperbolic resonant 2-tori, $p_{hyp}(h, -\alpha_1, I_2(h))$ and $p_{hyp}(h, I_1(h), -\alpha_2)$, belong to the circle of equi-energy normally hyperbolic 2-tori, $p_{hyp}(h, \cdot)$; hence, one is lead to the study of whiskered transition chains with resonant gaps, a subject which has received much attention in recent years (see [8, 45, 46]). Furthermore, as $(I_1, I_2) \to (-\alpha_1, -\alpha_2)$ we approach a double resonant hyperbolic torus - in this case the 3D figure corresponds to a revolution of the EMBD in fig. 8 around the starred line, with the strong resonant planes intersecting as in figure 4. Here the radius (in I) of the circle $p_{hyp}(h, \cdot)$ scales as $\sqrt{\varepsilon}$ (see fig. 8) hence the transition chain created near such a double resonant hyperbolic torus cannot create large instabilities. If the terms in I are indefinite near such a torus this situation may change (though our preliminary numerical simulations appear to indicate that even then the instability induced by the separatrices is not significantly enhanced [35]).

The doubly resonant elliptic tori $p^{\pm}_{ell}(h, -\alpha_1, -\alpha_2)$ reside on two small separate components of the energy surface hence cannot induce large instabilities.

Other cases corresponding to unbounded energy surfaces may be classified similarly.

6. Bifurcating systems

For n d.o.f. systems with $n \geq 3$ the appearance of parabolic resonant tori is persistent (see [35]), hence their study is both mathematically fascinating and physically relevant. Combining our understanding of the stable and unstable systems, we can now study H_{bif}:

$$H_{bif}(x,y,I_1,I_2) = \frac{y^2}{2} - \frac{x^2}{2}I_1 + \frac{x^4}{4} + (\mu_1 + \frac{1}{2})\frac{I_1^2}{2} + \frac{I_2^2}{2} + \alpha_2 I_2 + \alpha_3 I_1 I_2. \tag{6.1}$$

The phase space structure of the Hamiltonian H_{bif} for any fixed I is obvious - for $I_1 > 0$ it is given by the product of a figure eight motion in the xy plane and a family of 2-tori in the (θ, I) space as in H_{ust}, whereas for $I_1 < 0$ it corresponds to an elliptic motion around the origin in the xy plane and a family of 2-tori in the (θ, I) space as in H_{st}. At $I_1 = x = y = 0$ the system has a family of normally parabolic 2-tori. To understand the precise structure of each energy surface, we again construct the EMBD and the corresponding branched surfaces and then present the interesting energy surfaces in the frequency space.

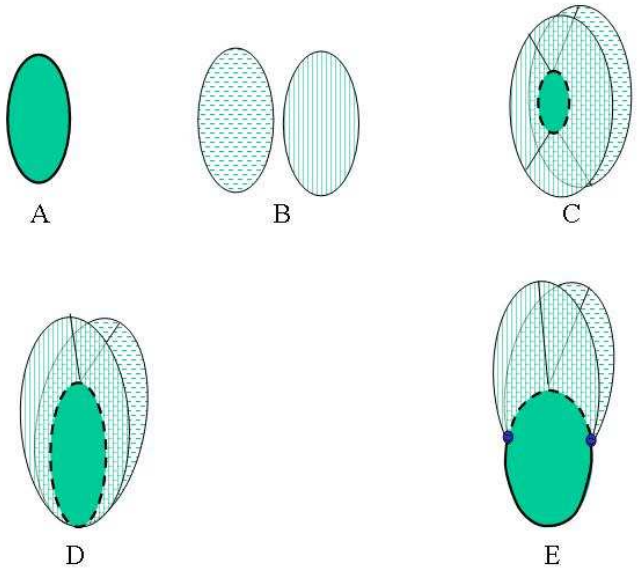

Figure 9. Generalized Fomenko graphs - the branched surfaces.

6.1. **Energy surfaces in the Energy-Momentum space (B).** Recall that the boundary of the allowed region of motion is composed of the singularity surfaces corresponding to lower dimensional normally elliptic tori. For (6.1), these are given

by the normally elliptic tori at $\{(x,y)=(\pm\sqrt{I_1},0);\ I_1>0\}$:

(6.2)
$$p^{\pm}_{ell}(h,I_1,I_2)=\left\{(h,I_1,I_2)|\ \mu_1\frac{I_1^2}{2}+\frac{I_2^2}{2}+\alpha_2 I_2+\alpha_3 I_1 I_2=h;\ h\geq h^{+}_{\min},I_1>0\right\}$$

and the elliptic tori at $\{(x,y)=(0,0);\ I_1<0\}$:

(6.3)
$$p^{0}_{ell}(h,I_1,I_2)=\left\{(h,I_1,I_2)\ |\ (\mu_1+\frac{1}{2})\frac{I_1^2}{2}+\frac{I_2^2}{2}+\alpha_2 I_2+\alpha_3 I_1 I_2=h;\ h\geq h^{0}_{\min},I_1<0\right\}.$$

Another surface of singularity, on which the hyperbolic tori $\{(x,y)=(0,0);\ I_1>0\}$ and their separatrices live is given by

(6.4)
$$p^{0}_{hyp}(h,I_1,I_2)=\left\{(h,I_1,I_2)\ |\ (\mu_1+\frac{1}{2})\frac{I_1^2}{2}+\frac{I_2^2}{2}+\alpha_2 I_2+\alpha_3 I_1 I_2=h;\ h\geq h^{0}_{\min},I_1>0\right\}.$$

Expressing the Hamiltonian on these surfaces in a quadratic form:

$$H_{bif}(0,0,I_1,I_2)=\frac{1}{2}(\mu_1+\frac{1}{2}-\alpha_3^2)\left(I_1-\frac{\alpha_2\alpha_3}{\mu_1+\frac{1}{2}-\alpha_3^2}\right)^2 + \frac{1}{2}\left(I_2+\alpha_2+\alpha_3 I_1\right)^2-\frac{1}{2}\alpha_2^2-\frac{1}{2}\frac{(\alpha_2\alpha_3)^2}{\mu_1+\frac{1}{2}-\alpha_3^2} \tag{6.5}$$

$$H_{bif}(\pm\sqrt{I_1},0,I_1,I_2)=\frac{1}{2}(\mu_1-\alpha_3^2)\left(I_1-\frac{\alpha_2\alpha_3}{\mu_1-\alpha_3^2}\right)^2 + \frac{1}{2}\left(I_2+\alpha_2+\alpha_3 I_1\right)^2-\frac{1}{2}\alpha_2^2-\frac{1}{2}\frac{(\alpha_2\alpha_3)^2}{\mu_1-\alpha_3^2} \tag{6.6}$$

shows immediately that the sign of $\mu_1-\alpha_3^2$ determines whether the energy surfaces are bounded or unbounded in I. Here, for simplicity and comparison with the previous cases, we present a bounded case. In particular, we hereafter assume:

$$\mu_1-\alpha_3^2>0,\qquad \alpha_2>0,\qquad 0<\alpha_3<1. \tag{6.7}$$

Other cases change some of the inequalities below, leading to a different EMBD and may be similarly analyzed - see for example [33, 32, 34, 35] where we considered mainly unbounded models. Here, equations (6.5) and (6.6) define paraboloids, and their intersections with the plane of constant energy define ellipses (see figures 10-16).

The minimal energies for which these paraboloids are defined are:

$$h^{+}_{\min}=-\frac{1}{2}\alpha_2^2-\frac{1}{2}\frac{(\alpha_2\alpha_3)^2}{\mu_1-\alpha_3^2}<h^{0}_{\min}=-\frac{1}{2}\alpha_2^2-\frac{1}{2}\frac{(\alpha_2\alpha_3)^2}{\mu_1+\frac{1}{2}-\alpha_3^2}, \tag{6.8}$$

with the corresponding minimizing actions:

$$(I_1,I_2)_{\min 0}=\left(\frac{\alpha_2\alpha_3}{\mu_1+\frac{1}{2}-\alpha_3^2},-\frac{\alpha_2\left(\mu_1+\frac{1}{2}\right)}{\mu_1+\frac{1}{2}-\alpha_3^2}\right)$$

$$(I_1,I_2)_{\min +}=\left(\frac{\alpha_2\alpha_3}{\mu_1-\alpha_3^2},-\frac{\alpha_2\mu_1}{\mu_1-\alpha_3^2}\right).$$

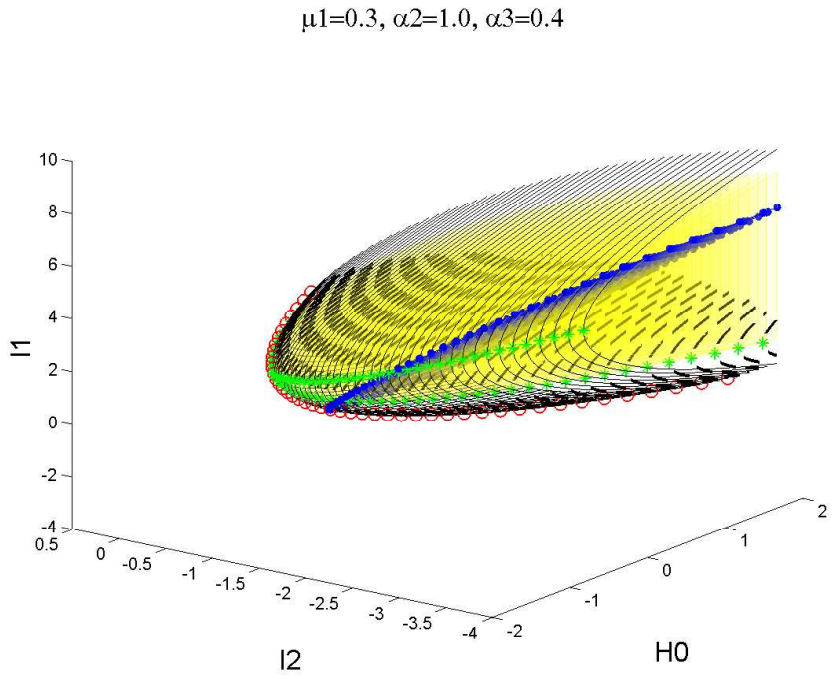

FIGURE 10. Energy-momentum bifurcation diagram for the bifurcating Hamiltonian, H_{bif}.

Finally, notice that the surface $I_1 = 0$ cuts the paraboloids $p^{\pm}_{ell}(h, I_1, I_2)$ and $p^0_{ell,hyp}(h, I_1, I_2)$ along a parabola which corresponds to a family of normally parabolic 2-tori:

$$p^0_{par}(h, I_1, I_2) = \left\{ (h, I_1, I_2) \mid I_1 = 0, \ \frac{I_2^2}{2} + \alpha_2 I_2 = h, \ h \geq h^p_{\min} \right\}, \tag{6.9}$$

where

$$h^p_{\min} = -\frac{1}{2}\alpha_2^2 > h^0_{\min}.$$

Let us now examine the appearance of strong resonances. Since

$$\omega_2(I_1, I_2) = \frac{\partial H_{bif}(x, y, I_1, I_2)}{\partial I_2} = I_2 + \alpha_2 + \alpha_3 I_1 \tag{6.10}$$

resonances in θ_2 (i.e., resonances in the direction of I_2) are given by the intersection of the domain of allowed motion with the plane

$$I_{2res} = -\alpha_2 - \alpha_3 I_1 \tag{6.11}$$

In particular, resonant lower dimensional tori appear when this plane intersects the paraboloids $p^0_{hyp}(h, \cdot)$, $p^0_{ell}(h, \cdot)$, $p^{\pm}_{ell}(h, \cdot)$ and $p^0_{par}(h, \cdot)$.

Due to the cross term $\frac{x^2}{2} I_1$ in H_{bif} (see eq. (6.1)) we cannot get such a simple and explicit expression for the θ_1-resonant tori surface $\omega_1(I_1, I_2) = 0$. However, the intersection of this surface with the singularity surfaces may be easily found -

the hyperbolic (resp. elliptic) lower dimensional tori $p^0_{hyp}(h,\cdot)$ (resp. $p^0_{ell}(h,\cdot)$) are resonant when $\omega^0_1 = 0$, where

$$\omega^0_1 = \frac{\partial H_{bif}(0,0,I_1,I_2)}{\partial I_1} = (\mu_1 + \frac{1}{2})I_1 + \alpha_3 I_2, \tag{6.12}$$

so resonance occurs exactly at the fold of the singularity surface in the I_1 direction. Hence, the intersection of the plane

$$I_{1res0} = -\frac{\alpha_3}{\mu_1 + \frac{1}{2}} I_2$$

with the paraboloid $p^0_{hyp}(h,\cdot) \cup p^0_{par}(h,\cdot) \cup p^0_{ell}(h,\cdot)$ corresponds to the family of lower dimensional resonant in the I_1-direction tori (the green starred curves in figure 10), $p^0_{res-1}(h,I)$. These tori are normally hyperbolic for $I_{1res} > 0$, normally elliptic for $I_{1res} < 0$ and, at $H_{bif} = h_{par-res1} = 0$, are normally parabolic (then $I_{1res} = I_2 = 0$). Similarly, the elliptic lower dimensional tori at $(x,y) = (\pm\sqrt{I_1}, 0)$, $p^{\pm}_{ell}$, are θ_1-resonant when $\omega^{\pm}_1 = 0$, where:

$$\omega^{\pm}_1 = \frac{\partial H_{bif}(\pm\sqrt{I_1},0,I_1,I_2)}{\partial I_1} = \mu_1 I_1 + \alpha_3 I_2.$$

Hence, the intersection of the plane

$$I_{1res\pm} = -\frac{\alpha_3}{\mu_1} I_2$$

with the paraboloids $p^{\pm}_{ell}(h,I_1,I_2)$, corresponds to these two families of normally elliptic lower dimensional resonant in the I_1-direction tori, $p^{\pm}_{res-1}(h,I)$ (denoted by green starred curves in figure 10 as well). The manifold of 3-tori, which are strongly resonant in θ_1, $p_{res-1}(h,I_1,I_2)$, intersects the paraboloids $p^0_{hyp}(h,\cdot) \cup p^0_{par}(h,\cdot) \cup p^0_{ell}(h,\cdot)$ and $p^{\pm}_{ell}(h,I_1,I_2)$ along the families $p^0_{res-1}(h,I)$ and $p^{\pm}_{res-1}(h,I)$.

Clearly, from the form of (6.1), strong resonance in the xy plane (namely, the normal frequency $\Omega = \omega_0(h,I_1,I_2) = 0$) may occur only at the parabolic tori $p^0_{par}(h,0,I_2) = p^0_{hyp}(h,0,I_2) = p^{\pm}_{ell}(h,0,I_2)$, where $\omega^{\pm}_0 = \sqrt{2I_1}$ and $\omega^0_0 = \sqrt{-I_1}$ vanish. Notice that here, at $I_1 = 0$, the natural frequency of the lower dimensional torus does vanish, as opposed to the formal definition of vanishing ω^0_0 which we had introduced for $I_1 > 0$.

In figure 10 a three dimensional EMBD of system (6.1) (Hamiltonian H_{bif}) is presented for typical parameter values, where the axis are the energy, H_0, and the actions, I_2 and I_1. The EMBD in this figure is plotted for a limited set of I_2 values to allow a glimpse into its complicated inner structure: the manifold of solid curves corresponds to the singularity manifold of elliptic 2-tori, $p^{\pm}_{ell}(h,I_1,I_2)$ and $p^0_{ell}(h,I_1,I_2)$, the manifold of dashed curves to hyperbolic 2-tori, $p^0_{hyp}(h,I_1,I_2)$, and the curve of red circles to parabolic 2-tori, $p^0_{par}(h,I_1,I_2)$; strongest resonance in the I_2 direction (where $\dot{\theta_2} = 0$ on the regular 3-tori or on the singular 2-tori) is denoted by a (vertical) blue surface of dotted lines and the 2-tori with the strongest resonance in the I_1 direction ($\dot{\theta_1} = 0$) by green starred curves. The yellow volume (or shaded regions in the 2D EMBD) corresponds to regular 3-tori on which $\dot{\theta_1}$ changes sign (back-flow). The surface of 3-tori which have strong resonance in the I_1 direction is contained in this region. The intersection of this surface with specific energy surfaces is calculated and is denoted by starred curves in the 2D slices of the EMBD - see figures 11A, 12A,C,D, 13A, 15 and 16; the tori with the

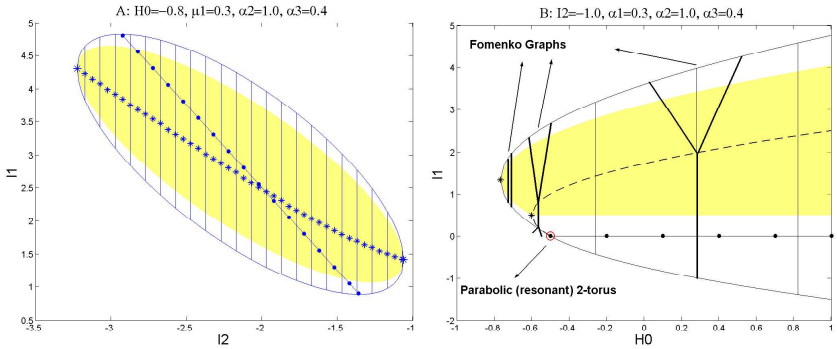

FIGURE 11. 2D slices of the EMBD of the bifurcating system, H_{bif}: A - an energy surface in the energy range: $h^{\pm}_{\min} < H_0 < h^0_{\min}$, B - an interval of energy values for a fixed value of $I_2 = -\alpha_2$ and all three possible types of (schematic) Fomenko graphs for H_{bif}.

strongest resonance in the I_2 direction are denoted in the 2D slices by a dotted line. The typical parameter values we choose for all EMBD plots presented here are: $\mu_1 = 0.3$, $\alpha_2 = 1$, $\alpha_3 = 0.4$; the corresponding bifurcation values for the energies are: $h^{+}_{\min} \approx -1.0714$, $h^0_{\min} = -0.625$, $h^p_{\min} = -0.5$ and $h_{par-res1} = 0$.

Below we describe the topological changes in the energy surfaces of system (6.1) and in the iso-energetic strong resonance structure as the energy is varied - namely, as one takes various 2D slices of figure 10. For energies in the range $H_0 = h$, $h^{+}_{\min} \leq h < h^0_{\min}$, the energy surfaces are composed of two separate components corresponding to oscillations in each of the potential wells (as in the low energy a priori unstable case). The energy surface in the EMBD is an ellipse, so any 2D section of figure 10 for this range of energies is similar to the EMBD slices of system H_{st} presented in figure 3; see for example the energy surface in figure 11A. The Fomenko graph for any one dimensional section of this ellipse is simply two segments - see figure 11B. Equivalently, the branched surfaces are two identical discs as in figure 9B, and the strong resonance surfaces $\omega_1(I_1, I_2) = \omega_2(I_1, I_2) = 0$ intersect the energy surface transversely, as shown by the starred and dotted lines in fig. 11A and schematically in fig. 14A. In particular, since the two resonant in the I_1 direction lower dimensional elliptic tori, $p^{\pm}_{res-1}(h, I_1, I_2)$, are separated along the circle $p^{\pm}_{ell}(h, I_1, I_2)$ by the two resonant in the I_2 direction lower dimensional elliptic tori, $p^{\pm}_{res-2}(h, I_1, I_2)$, it follows that the curves $p_{res-1}(h, I_1, I_2)$ and $p_{res-2}(h, I_1, I_2)$ of resonant 3-tori must intersect *at least* once in a double resonant 3-torus as shown schematically in figure 14A; indeed, a transverse intersection of the strongest resonance curves is depicted in figure 11A.

At $H_0 = h = h^0_{\min}$ a hyperbolic resonant bifurcation occurs, exactly as in the a priori unstable case; the singularity surface $p^0_{hyp}(h, I_1, I_2)$ appears in a 2-fold (since $I_{1\min 0} > 0$), creating a torus of fixed points which is normally hyperbolic - see figure 12A; the 2-resonant hyperbolic 2-torus is shown as a star ($\dot{\theta}_1 = \omega^0_1 = 0$) residing on the dotted line ($\dot{\theta}_2 = \omega_2 = 0$) - look *below* the starred curve, at the boundary of the yellow shaded region. In figure 12B the energy range $H_0 = h \geq h^0_{\min}$ is shown for the fixed value of $I_2 = I_{2\min 0}$ - the newly born 2-resonant hyperbolic torus appears

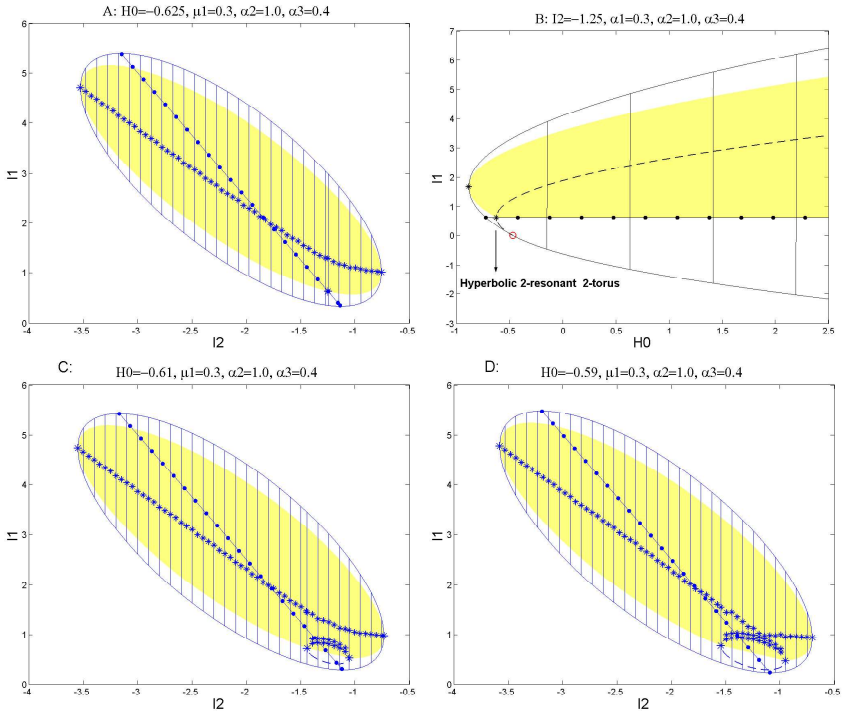

FIGURE 12. 2D slices of EMBD showing the energy range $h^0_{\min} \leq H_0 < h^0_p$: A - an energy surface corresponding to the energy value $H_0 = h^0_{\min}$, showing the hyperbolic bifurcation point, B - a range of energy values which includes the bifurcation value at which a hyperbolic double resonance occurs for a fixed value of $I_2 = I_{2\,\min\,0}$, C, D - energy surfaces containing the singular ellipse (dashed line) corresponding to hyperbolic 2-tori and their separatrices.

there in the fold of the dashed curve. The two disks of the branched surfaces meet exactly at this point (*unlike* in the a priori unstable case, where they connected at the cross of the two resonance curves $\omega_1 = \omega_2 = 0$, as shown schematically in figure 14B; while the topology of the energy surfaces is identical in these two cases, the topology of the strong resonances on the energy surfaces is different). For $H_0 = h$, $h^0_{\min} < h < h^p_{\min}$ we have, as before, a ring of I values for which two families of 3-tori, corresponding to oscillation in the wells, co-exists and a central region of I values for which only one family of 3-tori, corresponding to motion around the two wells exists. These regions are connected by an ellipse of I values, corresponding to normally hyperbolic 2-tori. Hence, for this range of energy values, the branched surface is a disk with two rings attached to it (figure 9C) and the energy surfaces in the EMBD are similar to the energy surfaces of H_{ust} in the hyperbolic energy range, as in figure 5A - see for example figure 12C,D.

Using the computation of $p^0_{res-1,2}(h, I)$, the *minimal number* of intersections of the strong resonance curves $p_{res-1}(h, I_1, I_2)$ and $p_{res-2}(h, I_1, I_2)$ in the interior disk is found to be one, as shown in fig. 14C. The 2D sections of figure 10 for these ranges

of energies demonstrate that for the bifurcating system (6.1) additional intersections appear (see fig. 12A,C,D); a bifurcation in the iso-energetic strong resonance curve $\omega_1 = 0$ occurs at $H_0 = h = h^0_{\min}$: for $h < h^0_{\min}$ this resonance curve is simple and smooth; at the bifurcation point $h = h^0_{\min}$ it splits to two components - a smooth curve of resonant 3-tori with two resonant elliptic 2-tori at its boundary and a resonant hyperbolic 2-torus as a separate component (see fig. 12A); for $h^0_{\min} < h < h^c_{\omega_1}$, the iso-energetic curve $\omega_1 = 0$ has three components: the smooth component of resonant 3-tori with elliptic resonant 2-tori as its boundary and the other two components, which reside above and below the ellipse of hyperbolic 2-tori and meet at the two resonant hyperbolic 2-tori, as seen in figure 12B. As the energy value increases, the components of $\omega_1 = 0$ approach each other until at the next bifurcation point of this curve, $H_0 = h = h^c_{\omega_1}$, all three components meet again (for the parameters chosen here $h^c_{\omega_1} \approx -0.59$ - see figure 13D), forming, for $h > h^c_{\omega_1}$, a one non-smooth component with cusp points at the resonant hyperbolic 2-tori, as seen in figure 13A (so the resonant surface $\omega_1 = 0$ folds in a shape of a nose looking towards the negative h values in the EMBD).

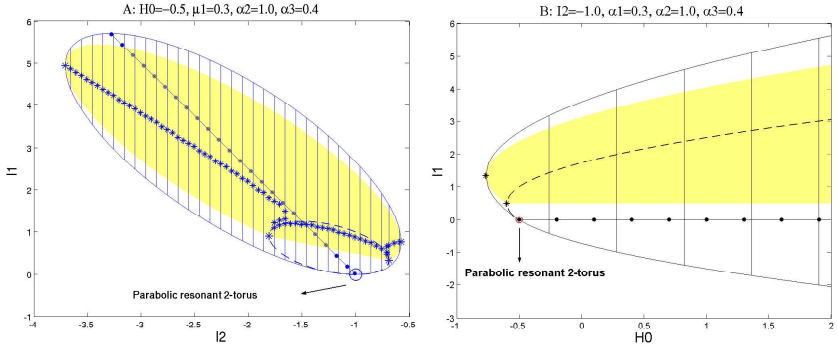

FIGURE 13. 2D slices of EMBD of the bifurcating system, H_{bif}, showing the parabolic bifurcation point: A - an energy surface corresponding to the energy value $H_0 = h^p_{\min}$, B - a range of energy values which includes the bifurcation value $H_0 = h^p_{\min}$ for a fixed value of $I_2 = -\alpha_2$.

At $H_0 = h = h^p_{\min}$ the ellipses $p^0_{hyp}(h^p_{\min}, \cdot)$ and $p^{\pm}_{ell}(h^p_{\min}, \cdot)$ touch the $I_1 = 0$ plane at $I_2 = -\alpha_2$, creating a parabolic torus (see the energy surface in the EMBD 13A and fig. 9D for a schematic representation). This bifurcation is, again, associated with a fold in the singularity surfaces in the EMBD and therefore with a resonance of a lower dimensional torus. Indeed, at $H_0 = h^p_{\min}$, the parabola $p^0_{par}(h, I_1, I_2)$ folds in the I_2 direction at $I_2 = -\alpha_2$, hence this parabolic 2-torus is resonant in θ_2:

$$\dot{\theta}_2\Big|_{(0,0,0,-\alpha_2)} = \frac{\partial H_{bif}(0,0,0,I_2)}{\partial I_2}\Big|_{I_2=-\alpha_2} = 0.$$

Furthermore, parabolicity of this torus implies that the torus is strongly resonant in the xy plane, namely $\omega^0_0 = 0$, so at $h = h^p_{\min}$ a double resonance occurs at the torus $(x, y, I) = (0, 0, 0, -\alpha_2)$. Figure 13 demonstrates the appearance of such a resonant parabolic torus for the system (6.1) (the dotted line in the figure, which denotes

resonance in the I_2 direction, intersects the boundary of allowed region of motion at the parabolic torus, which is denoted by a circle). The schematic representation of the branched surfaces with the resonant surfaces in figure 14C-D demonstrates that the first appearance of a parabolic torus occurs in a resonant parabolic torus.

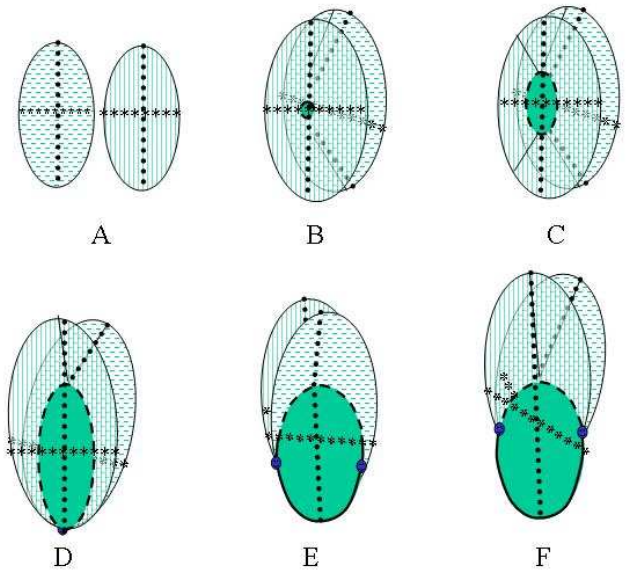

FIGURE 14. Energy branched surfaces and strong resonance curves.

In figure 15, 2D slices of the EMBD of system (6.1) for $H_0 = h > h^p_{\min}$ - energy surfaces in the (I_2, I_1) plane - are presented. For $h > h^p_{\min}$, the ellipse $H_{bif}(\pm\sqrt{I_1}, 0, I_1, I_2) = h$ is defined only for $I_1 \geq 0$ (the upper part of the bounding solid ellipses in fig. 15), and the ellipse $H_{bif}(0, 0, I_1, I_2) = h$ corresponds to hyperbolic tori for $I_1 > 0$ (the dashed part of the inner ellipses in fig. 15) and elliptic tori for $I_1 < 0$ (the lower solid part of the ellipses in fig. 15). Furthermore, there are exactly two parabolic tori on each energy surface (see eq. (6.9)); in figure 15 the two parabolic tori are denoted by circles and are seen at the meeting point of the different parts of the ellipses - solid (elliptic) and dashed (hyperbolic). The corresponding branched surface is a disk with two flaps emanating from it (see figure 9E), where the two end points of the flaps correspond to parabolic tori.

Now, consider the relative location of the resonant in the I_1 direction 2-tori, $p^0_{res-1}(h, I)$, and the parabolic 2-tori, $p^0_{par}(h, I)$ on the ellipse $H_{bif}(0, 0, I_1, I_2) = h$. For h values which are slightly larger than $h^p_{\min}$, this pair of resonant 2-tori live on the upper part of the ellipse, above the parabolic tori, hence they correspond to normally hyperbolic resonant 2-tori, as shown schematically in 14D. For such values of h the curve $p_{res-1}(h, I_1, I_2)$ intersects only the upper part of the ellipse (the dashed part of the ellipse in fig. 15A, corresponding to hyperbolic tori), so there are no resonant in the I_1 direction normally elliptic 2-tori at the origin (i.e., $p^0_{hyp}(h, I_1, I_2) \cap p_{res-1}(h, I_1, I_2) = \varnothing$), as shown in figure 15A. For energy values greater than $H_0 = h_{par-res1} = 0$ (i.e. for $h > h_{par-res1}$) this situation changes; for

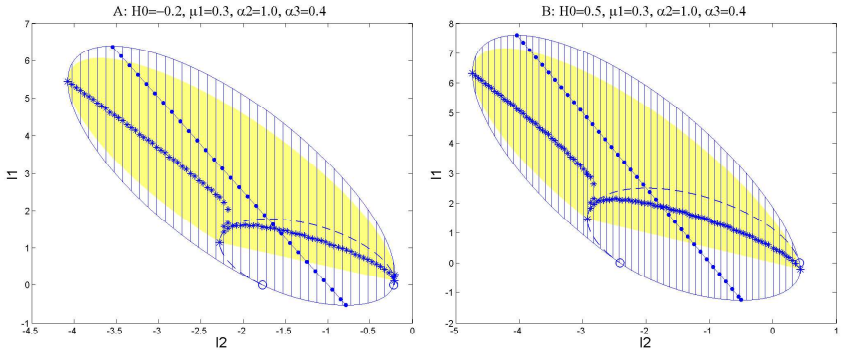

FIGURE 15. 2D slices of an EMBD of the bifurcating system, H_{bif}: A - an energy surface with $h^p_{\min} < H_0 < h_{par-res1}$, B - an energy surface with $H_0 > h_{par-res1}$.

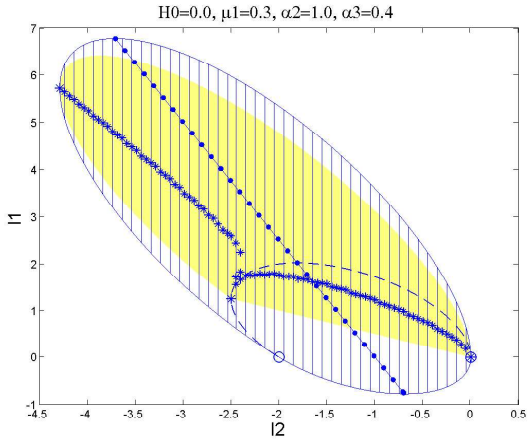

FIGURE 16. A 2D slice of EMBD of the bifurcating system, H_{bif} - an energy surface with $H_0 = h_{par-res1}$, containing a strongly resonant in the I_1 direction parabolic 2-torus.

$H_0 = h > h_{par-res1}$, the resonant plane $p_{res-1}(h, I_1, I_2)$ intersects each of the curves $p^0_{hyp}(h, \cdot)$ and $p^0_{ell}(h, \cdot)$ at one point (see the schematic figure 14F and the energy surface in figure 15B). Namely, one of the resonant hyperbolic lower dimensional tori, becomes normally elliptic for $H_0 = h > h_{par-res1}$. Therefore, at the bifurcation value, $H_0 = h_{par-res1} = 0$, the resonant plane in the I_1 direction intersects the ellipse $p^0_{hyp}(h, \cdot) \cup p^0_{par}(h, \cdot) \cup p^0_{ell}(h, \cdot)$ at $I_1 = I_2 = 0$, where a parabolic, resonant in the I_1 direction, lower dimensional torus is created (see schematic figure 14E,F). Indeed, in figure 16 it may be seen that at the bifurcation value, $H_0 = h_{par-res1} = 0$, one of the resonant hyperbolic tori changes it's stability and becomes parabolic (the end point of the starred curve, $\omega_1 = 0$, intersects one of the circles denoting a parabolic 2-torus; note that at the bifurcation point $H_0 = h_{par-res1}$, the iso-energetic curve $\omega_1 = 0$ ceases to have two cusp points and thereon has only one cusp point at

the remaining resonant hyperbolic 2-torus). Furthermore, in figure 17A a 2D slice of the EMBD at $I_2 = 0$ demonstrates that the resonance in the I_1 direction is indeed associated with a fold of the parabola $p^0_{hyp}(h, I_1, 0) \cup p^0_{par}(h, I_1, 0) \cup p^0_{ell}(h, I_1, 0)$ at the origin - the circle denoting the parabolic torus and the star denoting the strong resonance in the I_1 direction coincide.

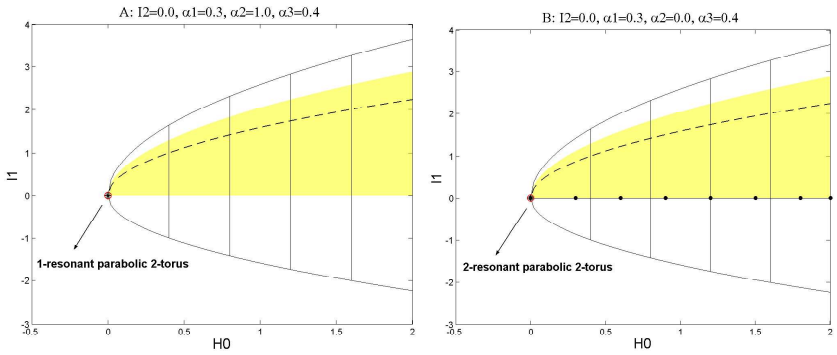

FIGURE 17. 2D slices of the EMBD at $I_2 = 0$: A - regular parameter values - at $I_1 = H_0 = 0$ a resonance in the I_1 direction occurs, B - at the special bifurcation value $\alpha_2 = 0$. Since $\alpha_2 = 0$, at $I_1 = H_0 = 0$ a double resonance in the I_1 and I_2 direction occurs.

Bifurcation values for the parameters are now easily identified. First, we see that at $\alpha_2 = 0$, $h^+_{\min} = h^0_{\min} = h^p_{\min} = h_{par-res1} = 0$, all the bifurcations mentioned above occur at one energy surface, and a double resonant (torus of fixed points in the 3 d.o.f. case) normally parabolic torus is created, as shown in figure 17B, where the star ($\omega_1 = 0$), the dotted line ($\omega_2 = 0$) and the circle (a parabolic torus) coincide; then, the energy surface $H_0 = \alpha_2 = 0$ of system (6.1) shrinks to one 2-resonant normally parabolic 2-torus of fixed points. The existence of a double resonant parabolic torus is a co-dimension one phenomena for 3 d.o.f. systems and a persistent phenomena in 4 or larger d.o.f. systems [35]. Normally parabolic tori of fixed points are a co-dimension one phenomenon for any $n \geq 2$ (see [41], [35] and [34] for more details).

Second, notice that

$$\frac{d^2 H_{bif}(\pm\sqrt{I_1}, 0, I_1, I_2)}{dI_1^2} = \mu_1$$

hence, the fold of the singular surface $p^+_{ell}(h, I_1, I_2)$ in the I_1 direction becomes flatter as $\mu_1 \to 0$ (put differently, the dependence of the frequency $\omega_1^{\pm}$ on I_1 becomes weaker). It is seen that holding α_3 fixed in this limit changes the character of the energy surfaces from being bounded to being unbounded in I_1, I_2. We will not delve into the analysis of all the different limits which may be taken here, and just note that the appearance of flat parabolic resonant tori in such situation gives rise to strong instabilities (see [35] and [34]).

6.2. **The frequency domain plots (B).** In the previous section we have established that the bifurcation values of the energy, where the geometrical properties of the energy surfaces are changed, are $h^+_{\min} < h^0_{\min} < h^p_{\min}$. At $h_{par-res1} = 0$ a lower

dimensional resonant torus changes its stability. Here, typical energy surfaces are chosen in each of the possible regions and presented in the frequency space and are denoted by ω^H. In addition, we present here the resonance web on some of these energy surfaces - to demonstrate its interesting structure (essentially different than the structure of the resonance webs of a priori stable systems). The parameters in all these plots are: $\mu_1 = 0.3$, $\alpha_2 = 1$ and $\alpha_3 = 0.4$, and we remind that the corresponding bifurcation values for the energies are: $h^+_{\min} \approx -1.0714$, $h^0_{\min} = -0.625$, $h^p_{\min} = -0.5$ and $h_{par-res1} = 0$.

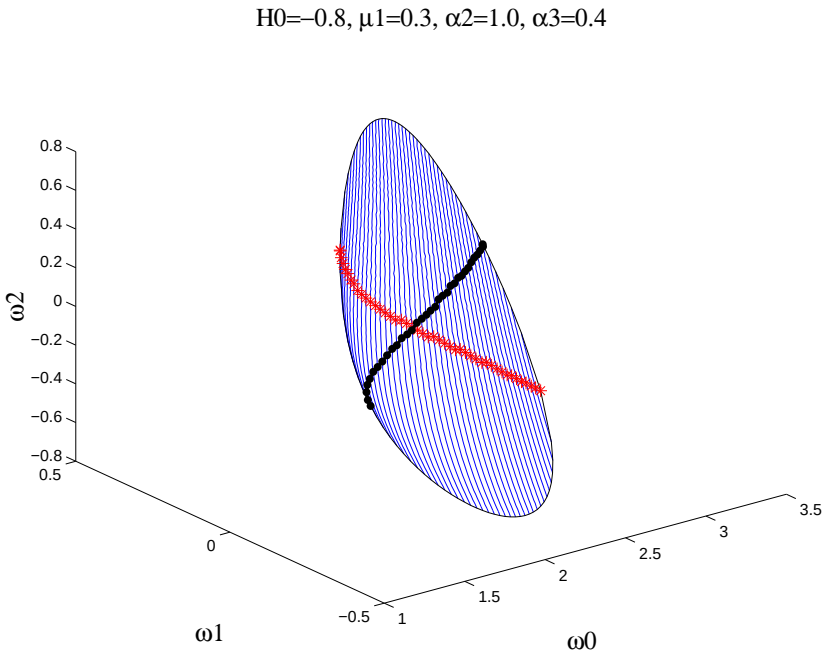

FIGURE 18. A typical energy surface corresponding to an elliptic energy value $H_0 = h$ with $h^+_{\min} < h < h^0_{\min}$.

The simplest type of energy surface component contains only elliptic lower dimensional tori. For $H_0 = h$, $h^+_{\min} < h < h^0_{\min}$ it appears as a smooth co-dimension one surface with boundaries, as shown in figure 18. Note the similarity to figure 6 where energy surface of the a-priori unstable system in the elliptic energy range is presented. This smooth compact component is a smooth deformation of the disk appearing in the energy-momentum space, (H_0, I_2, I_1). Transverse intersection of a smooth component of ω^H with one of the planes $\omega_j = 0$ corresponds to a strong resonance; for energy surfaces in the range $h^+_{\min} < h < h^0_{\min}$ this occurs only for $j = 1, 2$ (it cannot occur for $j = 0$ since in this energy range $\omega_0 > 0$). In figure 18 (and in the following figures here) the red starred curve corresponds to the intersection of the energy surface, ω^H, with the resonance plane, $\omega_1 = 0$, and the dotted line denotes the intersection of ω^H with $\omega_2 = 0$. The lower dimensional elliptic resonant tori correspond to the intersections of the surfaces' boundary with the $\omega_j = 0$ ($j = 1$ or 2) planes.

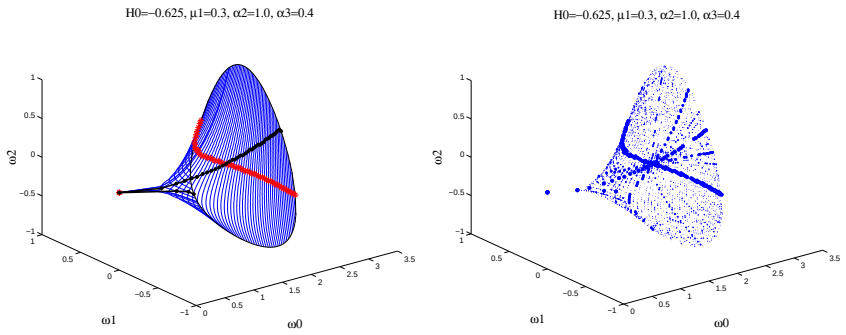

FIGURE 19. An energy surface corresponding to the bifurcation value $H_0 = h^0_{\min}$, containing a double resonant hyperbolic torus of fixed points: left - the frequency map plot, right - the resonance web on this energy surface for $|k| \leq 21$, where the size of the dots indicate the strength of the resonance.

The energy value $H_0 = h^0_{\min}$ is a bifurcation value at which one 2-resonant hyperbolic 2-torus (hyperbolic torus of fixed points) appears. It creates a singular cusp point in the energy surface ω^H - see figure 19, where this energy surface is presented in the three frequency space in the left plot (each blue thin curve corresponds to a fixed value of I_2, the red starred curve to the strong resonance $\omega_1 = 0$ and the black dotted line to the strong resonance $\omega_2 = 0$) and the resonance web on this energy surface is presented in the right plot. The resonance webs presented here are calculated by finding (approximately) the points on the energy surface for which $\langle k, \omega^H \rangle = 0$ for $0 < |k| = |k_1| + |k_2| + |k_3| \leq 21$, where the size of the dots is in inverse relation to $|k|$ - i.e. the stronger the resonance the larger the dot indicating it (note that for the weaker resonances the difference in the size of the dots is indistinguishable). It may be seen that the hyperbolic 2-resonant 2-torus in fig. 19 resides in the cusp, far from where other resonance surfaces intersect this energy surface; in particular, it resides far from the main resonance junction on this energy surface, where strong resonances intersect (this might suggest an additional reason for not observing strong instabilities of the perturbed system near such hyperbolic double resonance [35]).

Energy surfaces with $H_0 = h$, $h^0_{\min} < h < h^p_{\min}$, include a circle of hyperbolic tori with their separatrices. As for the a-priori unstable case, we find that the energy surface ω^H collides at this singular circle with the plane $\omega_0 = 0$, and then bounces back with the same sign of ω_0 (since the direction of motion does not change from the exterior to the interior tori). Using equations (6.12) and (6.10) we find that the singularity manifold corresponding to the family of hyperbolic 2-tori is given by

$$\begin{aligned} H_{bif}(0,0,I_1,I_2) &= H_{bif}(0,0,\omega_1,\omega_2) = \\ &= \frac{1}{2}\frac{\left(\omega_1^0 - \alpha_3\omega_2\right)^2}{\mu_1 + \frac{1}{2} - \alpha_3^2} + \frac{1}{2}\left(\omega_2\right)^2 - \frac{1}{2}\alpha_2^2 - \frac{1}{2}\frac{\left(\alpha_2\alpha_3\right)^2}{\mu_1 + \frac{1}{2} - \alpha_3^2} \end{aligned} \tag{6.13}$$

For our parameter range it is a tilted ellipse, lying in the $\omega_0 = 0$ plane which is centered at the origin, as can be seen in figure 20 (note similarity to figure 7).

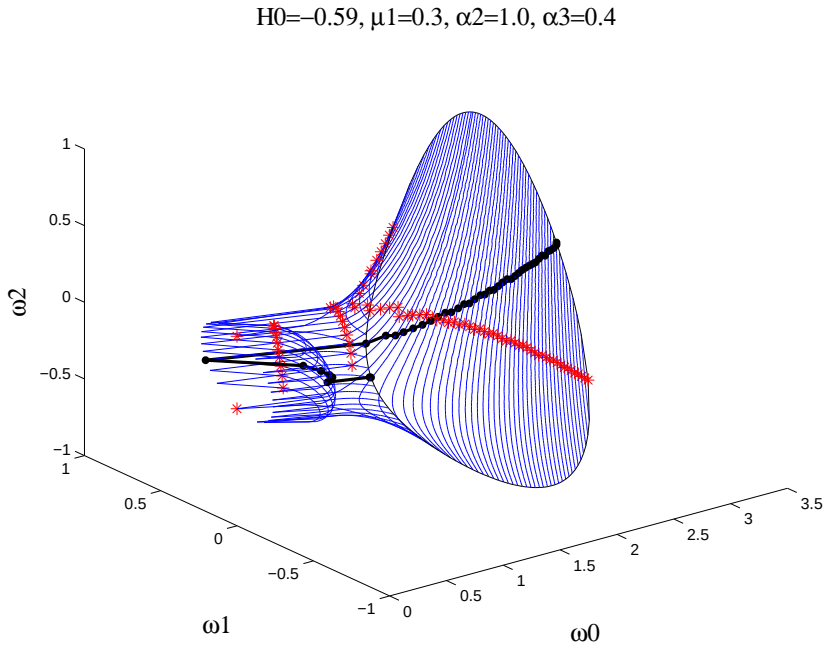

FIGURE 20. A typical energy surface in the hyperbolic energy range, corresponding to an energy value $H_0 = h$ with $h^0_{\min} < h < h^p_{\min}$.

On one side of this singularity manifold each point on the energy surface corresponds to two 3-tori, and on the other side to a single 3-torus as summarized by figure 9C. Each of the surfaces $\omega_j = 0$ $(j = 1, 2)$ intersects the ellipse at two points, at hyperbolic 1-resonant 2-tori. In [35] we prove that such intersections are persistent. Recall that even though the singular circle is contained in the $\omega_0 = 0$ plane it does not correspond to a double resonance of the lower dimensional torus: $\omega_0 = 0$ at the homoclinic loop, whereas the normal frequency of the hyperbolic torus is imaginary and is non-zero.

At the bifurcation value $H_0 = h^p_{\min}$ a parabolic (resonant in the I_2 direction) torus first appears - see figure 21. An important observation is that *parabolic tori are a priori resonant*: their normal frequency vanishes. Indeed, let $\omega = (\Omega, \omega^{n-1}) \in \mathbb{R}^n$ denote the n dimensional vector of frequencies, including the normal frequency Ω, and the inner frequencies $(\omega^{n-1} \in \mathbb{R}^{n-1})$ of the $(n-1)$-torus. Parabolicity implies $\Omega = 0$, hence, $k^1 = e^1_n = (1, 0, ..., 0)$ satisfies the resonance condition $\langle k^1, \omega \rangle = 0$ (indeed, in the resonance web plots a large dot indicating strongest resonance always appears on the parabolic tori - see e.g. fig. 21). Lower dimensional resonance implies that there exists at least one additional vector of integers, $k^2 = (0, l_{n-1}), l_{n-1} \in \mathbb{Z}^{n-1}$, such that $\langle k^2, \omega \rangle = 0$. Hence, *parabolic lower dimensional resonant tori correspond to junctions in the resonance web with at least one strongest resonance* (indeed, the parabolic torus in fig. 21 is doubly resonant, residing on the junction $\omega_0 = \omega_2 = 0$). In particular, if the parabolic torus appears at the

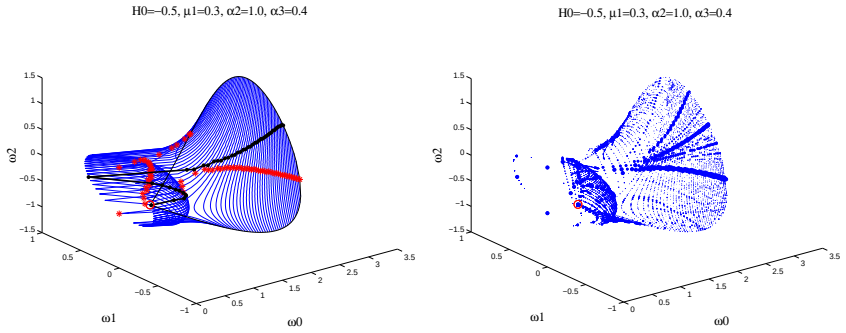

FIGURE 21. An energy surface with $H_0 = h^p_{\min}$: left - the energy surface in the frequency space, right - the resonance web on this energy surface. Red circle - (double) resonant (in the I_0 and I_2 directions) parabolic 2-torus.

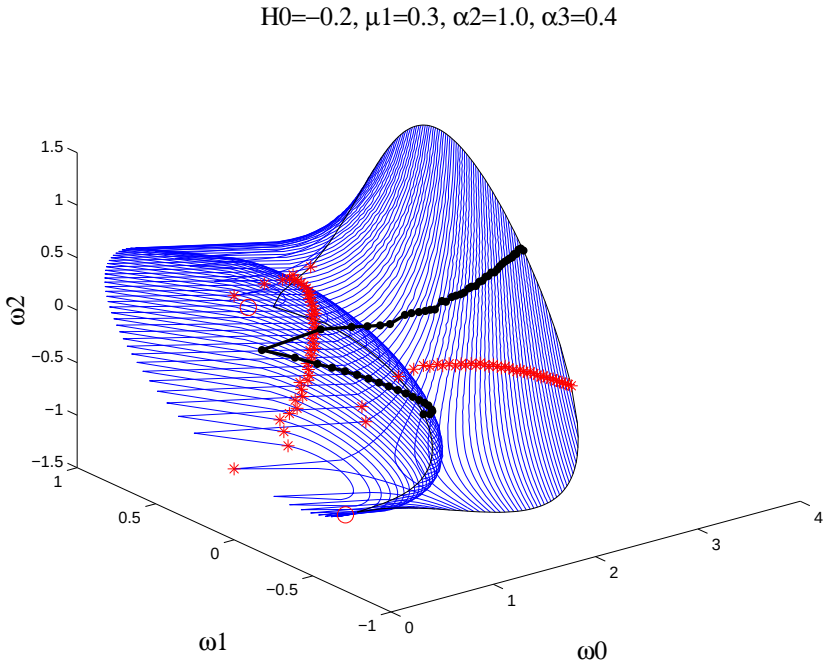

FIGURE 22. A typical energy surface with $h^p_{\min} < H_0 < 0$.

origin, where all resonances intersect, it corresponds to $(n-1)$-resonant $(n-1)$-torus, namely to a parabolic torus of fixed points. In [35] we prove that such a scenario is persistent in a one parameter family of integrable n d.o.f. Hamiltonian systems with $n \geq 2$.

A typical energy surface in the energy range $H_0 = h$, $h^p_{\min} < h < h_{par-res1} = 0$ is shown in figure 22 and in the range $H_0 = h > h_{par-res1} = 0$ in figure 23, where the two parabolic tori are denoted by red circles. Then, the natural frequency in

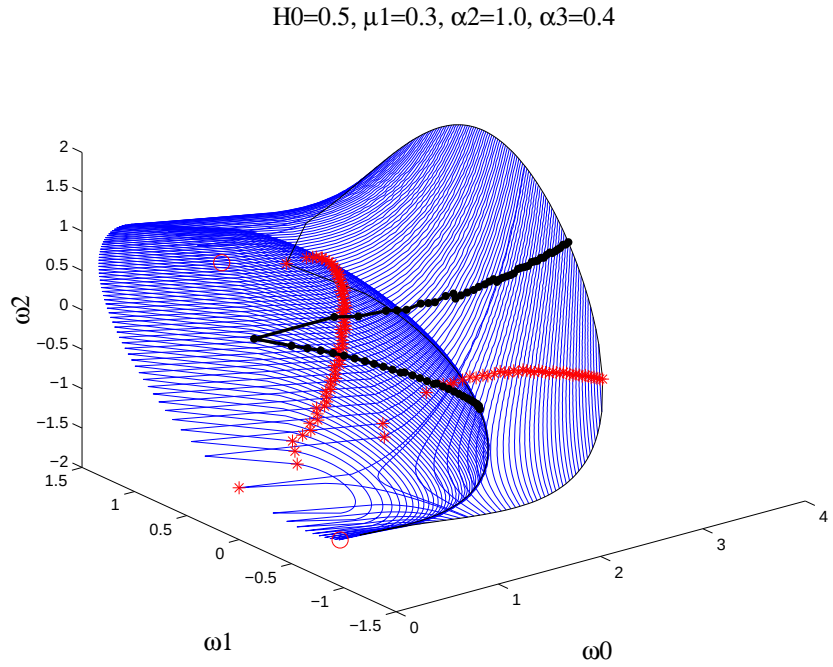

FIGURE 23. A typical energy surface in the range $H_0 > h^0_{par-res1} = 0$.

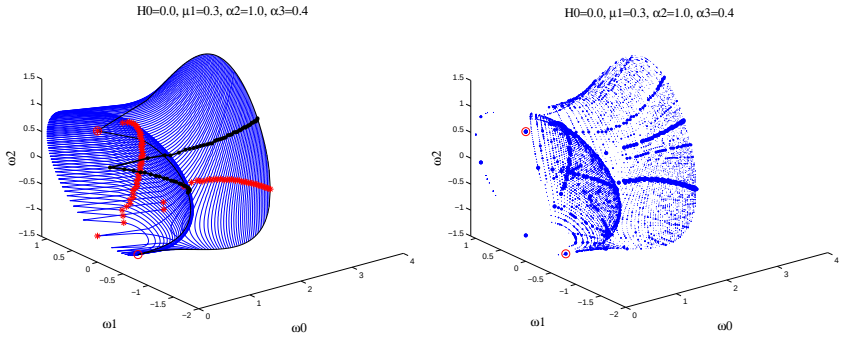

FIGURE 24. An energy surface with $H_0 = h_{par-res1} = 0$, containing a strongly resonant in the I_1 direction parabolic 2-torus (hence, a double resonant parabolic torus): left - this energy surface in the frequency space, right - the resonance web on this energy surface.

the xy direction found from linearization at the origin:

$$\omega_0^0 = \sqrt{-I_1} = \sqrt{\frac{\omega_1^0 - \alpha_3\omega_2}{\mu_1 + \frac{1}{2} - \alpha_3^2} - \alpha_2\alpha_3}$$

shows that the singularity ellipse (eq. (6.13)) detaches from the $\omega_0 = 0$ plane with a square-root distance. Topologically, the energy surface is well described by the branched surface in figure 9E.

The colliding surface, at which ω^H is singular (non-smooth), is clearly of co-dimension two, and it corresponds to the family of hyperbolic tori which live on the given energy surface. The end points of this collision surface, where the projection singularity heals and the energy surface cease to contain hyperbolic tori, corresponds to parabolic tori, a co-dimension 3 surface, namely points in figures 9, 21, 22, 23 and 24 (the parabolic tori are denoted by red circles). At the parabolic lower dimensional tori the ω_0 frequency vanishes. If such an end surface (in the figures, a point) intersects another resonance surface a parabolic (doubly) resonant torus is born. It is now clear that with additional d.o.f. such an intersection (of the boundary of the collision surface and the resonances on the $\omega_0 = 0$ plane) is generically transverse (see [35] for a proof), hence parabolic resonances (PR) are expected to occur on surfaces corresponding to a range of energies. For the 3 d.o.f. case, since generically the end points (corresponding to the inner frequencies of the parabolic tori) change continuously with the energy values, there exists a set of dense values of energies for which these end points hit resonance surfaces and PR are created. When an end point of a singularity curve belongs to a strong resonance plane $\omega_j = 0$ ($j = 1$ or 2) it corresponds to a strong *double resonance* of the parabolic lower dimensional torus (see the resonance webs in figures 21 and 24).

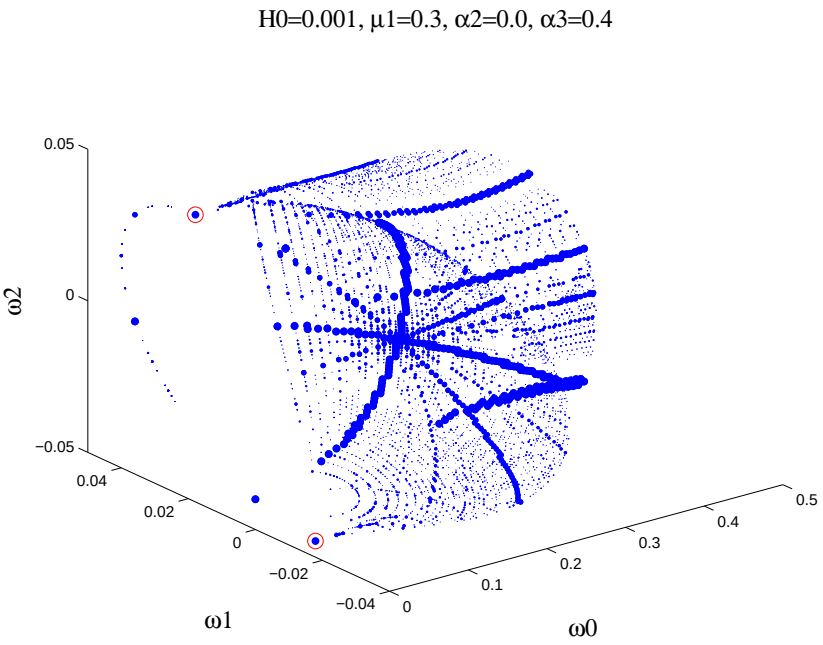

FIGURE 25. A resonance web on an energy surface near the (locally KAM degenerate) energy surface with $H_0 = \alpha_2 = 0$.

Figure 23 shows an energy surface for positive H_0, were the family of tori encircling the two wells crosses the $\omega_1 = 0$ plane. Figure 24 shows an energy surface

with $H_0 = h_{par-res1} = 0$, which contains a resonant in the I_1 direction parabolic torus (hence strongly doubly resonant with $\omega_0 = \omega_1 = 0$) and the resonance web on this energy surface. Setting (in addition) $\alpha_2 = 0$, the energy surface with $H_0 = 0$ shrinks to a parabolic torus of fixed points at the origin of the frequency space. However, near by energy surfaces (i.e. energy surfaces with $\alpha_2 = 0$ and a small energy value) have a non-diminishing extent in the frequency space, with resonant parabolic 2-tori residing near the main junction where many strong resonances intersect - see figure 25 (note the scale of the axis).

Summarizing, we discovered that the presentation in the frequency space of the energy surfaces of Hamiltonians of the form $H_0(x, y, I)$ with $n-1$ dimensional tori that change their stability has the following properties:

- For a range of energies, the energy surface is singular along a co-dimension 2 surface belonging to the $\omega_0 = 0$ plane. This singularity surface corresponds to hyperbolic lower dimensional tori and their separatrices. The boundaries of the singularity surface (of co-dimension 3) correspond to parabolic tori.
- Parabolic resonant tori may be recognized as resonance junctions which belong to the boundary of the hyperbolic singular surface. For 3 d.o.f. systems these appear on a dense set of energy values, for $n \geq 4$ these appear for a range of energies.
- While the resonance surfaces still intersect the energy surfaces densely, the *uniformity seems to be lost.*
- Parabolic torus of fixed points appears when the boundary of the singular surface contains the origin. Such a scenario appears for special parameter values (a co-dimension one phenomena), and on specific energy surfaces.

6.3. **Qualitative behavior of the near-integrable system (B).** Using the plots of the EMBD we may read off all possible sources of instabilities. Here we need to combine several effects:

- Instabilities associated with the regular resonance web, as in the elliptic case.
- Instabilities associated with the existence of equi-energy family of separatrices and their resonances, as in the unstable case.
- Instabilities associated with resonant parabolic tori; their appearance implies the co-existence of equi-energy families of separatrices and equi-energy families of lower dimensional elliptic tori, meeting at the parabolic tori.
- Instabilities associated with bifurcations in the structure of the singularity manifolds (manifolds corresponding to lower dimensional tori) of the energy surfaces - namely the creation of elliptic, hyperbolic and parabolic lower dimensional tori, all of which are associated with resonant lower dimensional tori.

Once again, the detailed analysis of each of the above items is not yet understood. For the parabolic case we have mainly numerical indications for the behavior of the perturbed orbits. The behavior near non-resonant parabolic torus is not very interesting - the lower dimensional parabolic torus persists [23] - and it appears that the behavior near it is not distinguishable from that appearing near lower dimensional normally elliptic torus. However, numerical simulations indicate that the behavior near PR is dramatically different - orbits which appear to be chaotic and of different nature then the homoclinic chaos are abundant. The structure of

these perturbed orbits near 1-PR, which appear for a dense set of energy values, is similar to the one observed in the 2 d.o.f. case, see [34], [41]. Further degeneracies make the instabilities more pronounced, see [34, 35] for examples.

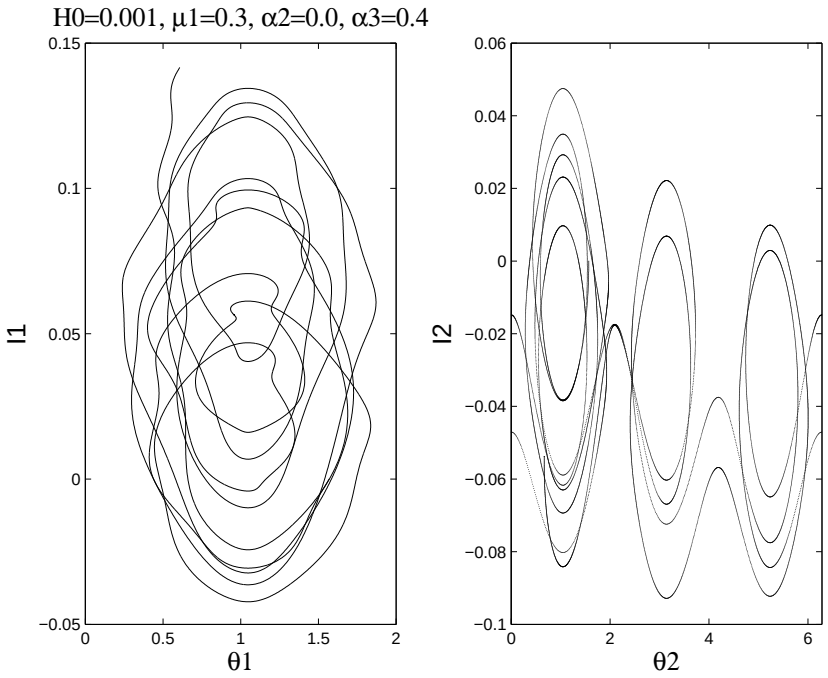

FIGURE 26. Instability in the action variables near 2-PR: a perturbed orbit projected on the (θ, I) planes, corresponding to the total energy $H \approx 9.953e-4$, with initial conditions: $(x, y, \theta_1, I_1, \theta_2, I_2; \varepsilon) = (0.2515, 0, 1.57, 0, 1.57, 0, 1e-3, 1e-3)$.

One degeneracy we explore here is the existence of a normally parabolic torus of fixed points, which is of co-dimension one ($\alpha_2 = 0$), and corresponds to *a local* violation of the KAM non-degeneracy condition. The induced strong instabilities of a perturbed orbit with initial values near this point is presented in figures 26 and 27; in figure 26 the perturbed orbit is projected on the (θ, I) planes, where it's complicated structure, while it passes through the successive resonance zones may be seen; in figure 27 we show the development of the instabilities in the action variables depending on time. These figures were produced for the perturbed Hamiltonian:

(6.14)

$$H^{\varepsilon}_{bif}(x, y, \theta_1, I_1, \theta_2, I_2; \varepsilon) = \frac{y^2}{2} - \frac{x^2}{2} I_1 + \frac{x^4}{4} + (\mu_1 + \frac{1}{2})\frac{I_1^2}{2} + \frac{I_2^2}{2} + \alpha_3 I_1 I_2 + \\ + \varepsilon((1 - \frac{x^2}{2})\cos(3\theta_1) + \cos(3\theta_2)).$$

Graphically, in the frequency space, such a scenario happens when the boundary of the singularity surface (here the end points of the singularity lines) passes through

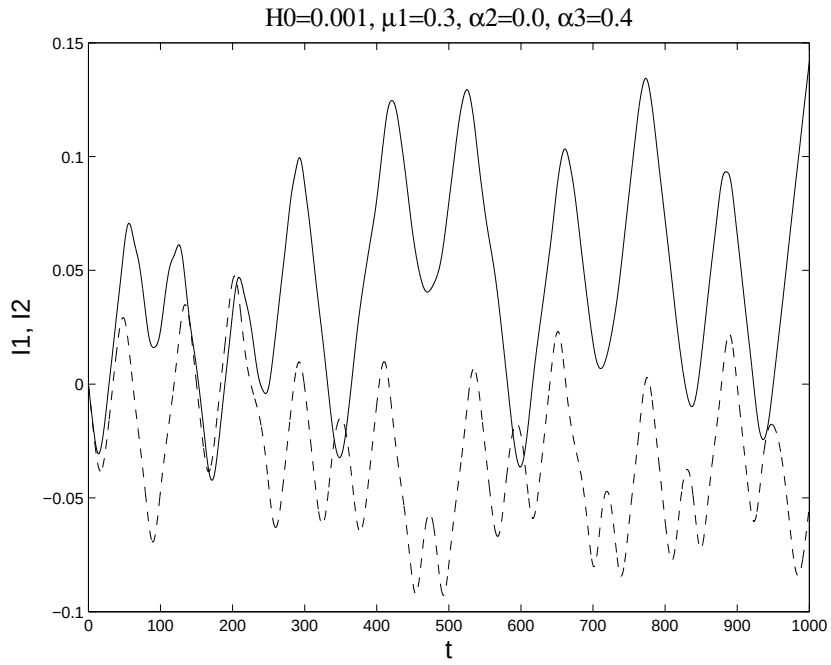

FIGURE 27. Instability in the action variables near 2-PR: a perturbed orbit projected on the time-actions plane, with initial conditions as in figure 26.
Solid line: I_1, Dashed line: I_2.

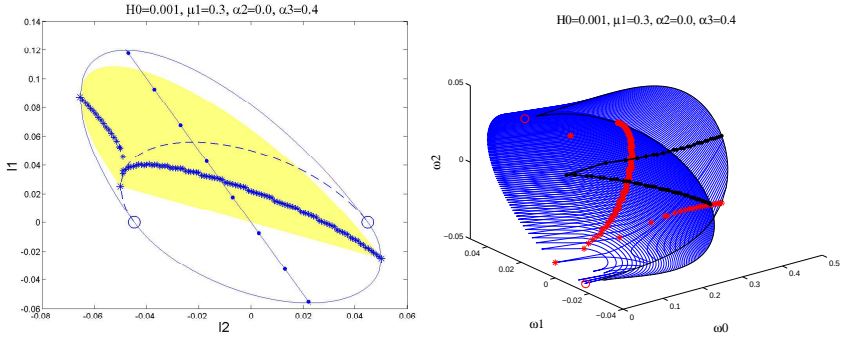

FIGURE 28. An energy surface of H_{bif} with $\alpha_2 = 0$, $H_0 = 1e-3$: left - an EMBD in the (I_2, I_1) plane, right - in the frequency space.

the origin, where all the resonance planes intersect. The fact that a parabolic 2-resonant torus resides at this junction point seems to induce strong instabilities in the perturbed system in both action directions, as seen in figures 26 and 27. In figure 28 the corresponding unperturbed energy surface is shown in the (I_2, I_1) plane and in the frequency space (see the corresponding resonance web in fig. 25). The perturbed orbit shown in figures 26 and 27 approximately covers the whole

possible extent of the actions range on this surface (for more details and upper bounds on the maximal instability rate see [34, 35]).

Note that in 4 or more d.o.f. systems the existence of a double resonant parabolic torus is persistent without dependence of the system on external parameters, and the local violation of the KAM iso-energetic non-degeneracy condition is avoided. Numerical simulations suggest that near such double PR the instabilities and the orbit structure are similar to the ones appearing in the locally degenerate 3 d.o.f. system (with $\alpha_2 = 0$).

7. Bifurcations in the energy-momentum diagrams

Here we formulate the observed relations between bifurcations in the EMBD and the appearance of lower dimensional resonances precisely. First we prove that extrema of the non-parabolic singularity surfaces in the EMBD occur iff the corresponding tori are resonant. Then we address questions regarding changes in the energy-surface topology. We define precisely what are the generalized branched surfaces, define topological bifurcations as energies for which the topology of the branched surfaces changes, and then prove that non-degenerate strong $(n-1)$-resonances of an $(n-1)$-non-parabolic torus imply topological changes. We end with formulating similar results for the parabolic case. After stating the results for the generic parabolic case we discover that our model Hamiltonian H_{bif} is non-generic in this context and formulate the corresponding results to a suitable class of Hamiltonians.

7.1. **Folds in the EMBD and Resonances.** Consider the EMBD near a singular family of $n-1$ lower dimensional tori, p_f (here we again take $s = 1$. General value of s will be considered elsewhere). The unperturbed Hamiltonian, expressed in suitable local Arnold-Liouville-Nekhoroshev coordinates near p_f is given by $H_0 = H_0(x, y, I)$, where $p_f = (x_f, y_f, I_f)$ satisfies $\nabla_{x,y} H_0(x, y, I)|_{p_f} = 0$. By the Implicit Function Theorem (IFT), if the Hessian of H_0 with respect to x, y is non-singular at p_f (namely $\det \frac{\partial^2 H(x,y,I)}{\partial x \partial y}\Big|_{p_f} \neq 0$), we may express this manifold as a graph over the I variables: $p_f = (x_f(I), y_f(I), I)$. Then, apart of parabolic points (where $\det \frac{\partial^2 H(x,y,I)}{\partial x \partial y}\Big|_{p_f} = 0$), p_f is represented in the EMBD by the co-dimension one smooth manifold $p_f^h = \{h_f(I), I\} = \{H_0(x_f(I), y_f(I), I), I\}$ [8]. It is now natural to define extremal points of the singularity surface in the EMBD:

Definition 2. *p_f^c is a simple $k-$extremal point of the singularity manifold p_f^h if p_f^c is non-parabolic and $h_f(I) = H_0(x_f(I), y_f(I), I)$ has a local extremal in k directions at p_f^c; i.e. there exist $i_1, ..., i_k \in \{1, ..., n-1\}$ such that*

$$\frac{\partial h_f(I)}{\partial I_i}\Big|_{p_f^c} = 0 \text{ for } i = i_1, ..., i_k. \tag{7.1}$$

Theorem 1. *Consider a family of singular non parabolic $n-1$ dimensional tori $p_f(I) = (x_f(I), y_f(I), I)$, where (x, y, I) are suitable coordinates near $p_f(I)$. Then $p_f^c = p_f(I^c)$ is a simple $k-$extremal point of the corresponding singularity manifold in the EMBD iff p_f^c corresponds to a $k-$strongly resonant lower dimensional torus.*

[8] With a slight abuse of notation we denoted it in previous sections by $p_f = (h_f(I), I)$ as well (see for example equations (6.2), (6.3), (6.4))

Proof. Since p_f^c is not parabolic the representation $p_f^h = \{h_f(I) = H_0(x_f(I), y_f(I), I), I\}$ is non-singular near p_f^c. Hence, p_f^c is a k-extremal point iff the surface $\{h_f(I) = H_0(x_f(I), y_f(I), I), I\}$ in the (h, I) space is extremal in k directions $I_{i_1}, ..., I_{i_k}$ at p_f^c. This occurs, by definition, iff $\frac{\partial h_f(I)}{\partial I_i}$ vanishes in the corresponding k directions at p_f^c as expressed in eq. (7.1). Since we use suitable coordinates, and since $\nabla_{x,y} H_0(x, y, I)|_{p_f} = 0$, it follows that for $i = i_1, ..., i_k$:

$$\dot{\theta}_i\Big|_{p_f^c} = \frac{\partial H(x, y, I)}{\partial I_i}\Big|_{p_f^c} = \frac{dH(p_f(I))}{dI_i}\Big|_{p_f^c} = \frac{\partial h_f(I)}{\partial I_i}\Big|_{p_f^c} = 0. \tag{7.2}$$

□

Theorem 1 relates extremal point of the singularity surfaces in the EMBD and resonances. We have seen that the topology of the energy surfaces changes at folds of these singular surfaces. We remind here the triviality that folds imply extremum points and extremum points with first non-vanishing derivatives of even order imply folds.

7.2. **Generalized branched surfaces.** In the previous section we saw that H_{bif} has two values $h_c = h_{ell}^+, h_{hyp}^0$ which are simple 2-fold points of the elliptic and hyperbolic singularity surfaces (namely these singularity surfaces have an even order extrema in two action directions), several families of curves on which simple 1-fold occurs (corresponding to the intersection of the singularity surfaces $p_{ell}^{\pm}, p_{hyp}^0, p_{ell}^0$ with the corresponding resonances) and $h_c = h_p^0$ is a 1-parabolic fold point corresponding to the first appearance of parabolic tori. We observe that h_{ell}^+, h_{hyp}^0 and h_p^0 correspond to a topological change in the energy surfaces structure, namely, the corresponding topology of the branched surfaces changes across these energy values, but that the families along which a simple 1-fold occurs do not correspond to such changes. We would like to formulate these observations. First, we need to define the branched surfaces in a precise way.

Consider an integrable n d.o.f. Hamiltonian on a $2n$ dimensional symplectic manifold M, and its associated n integrals of motion $H_0 = F_1, F_2, ..., F_n$. We call the set of constants of motion *valid* if they are *almost everywhere* independent on M (i.e. the dF_i are linearly independent on M) and are pair-wise in involution. Denote by A_h the set of allowed values of $F_2, ..., F_n$ on the energy surface $E_h = \{(q,p)|\ H_0(q,p) = h\}$, namely, $A_h = \{(g_2, ...g_n)|\ M_{(h,g_2,...g_n)} \neq \emptyset\}$ (recall that the level set M_g is defined as $M_g = \{(q,p) \in M, \quad F_i = g_i; \quad i = 1, ..., n\})$. It follows that $E_h = \cup_{(g_2,...g_n) \in A_h} M_{(h,g_2,...g_n)}$. Let $k(g)$ denote the number of disconnected components of M_g, so $M_{(h,g_2,...g_n)} = \biguplus_{j=1}^{k(h,g_2,...g_n)} l_j^{(h,g_2,...g_n)}$ where l_j^g denotes a connected component of M_g. Fixing h, $k(h, g_2, ...g_n)$ is constant when the level sets $M_{(h,g_2,...g_n)}$ deform smoothly with $g_2, ...g_n$. Recall (see section 2) that the singularity surfaces of A_h are defined as the values of $(g_2, ...g_n)$ for which there exist a point $(q,p) \in M_{(h,g_2,...g_n)}$ at which s of the dF_i are linearly dependent and the rank of the n vectors dF_i at the singularity is denoted by $n - s$. Let us denote the union of the singularity surfaces of some given A_h by A_h^S. Clearly, $k(h, g_2, ...g_n)$ may change only across a singular level set, hence:

$$A_h^S \supseteq A_h^{GS} = \{(g_2, ...g_n)|\ k(h, g_2, ...g_n) \text{ is discontinuous in } g_2, ...g_n\}.$$

Equality of these sets is expected in the generic case with $s = 1$. Non-generic (e.g. symmetric) coincidences, by which disconnected level sets coincide and split at the same g value may be similarly treated and will be ignored here (see [17] and [30] for discussion). The behavior of $k(h, g_2, ...g_n)$ near singular level sets with $s \geq 2$ will be studied elsewhere.

Define a function $S_h : E_h \to \mathbb{R}^n$ as follows (recall that $g_1 = h$):

$$S_h(q,p) = (\delta(q,p), g_2, ...g_n), \text{ where } F_i(q,p) = g_i,\ i = 1, ..., n$$

where the scalar function $\delta(q,p)$ satisfies:

- $\delta(q,p) = 0$ iff $k(g(q,p)) = 1$,
- Two points belonging to the same level set have the same δ iff they belong to a connected component of M_g :

$$\{(q,p),(q',p') \in M_g \text{ and } \delta(q,p) = \delta(q',p')\} \Leftrightarrow (q,p),(q',p') \in l_j^g$$

- $\delta(q,p)$ is smooth (C^r) for all $(q,p) \in E_h$ with $(g_2, ...g_n) \in A_h \backslash A_h^S$ and $\delta(q,p)$ is continuous for $(g_2, ...g_n) \in A_h$.

It follows that $\delta(q,p)$ attains exactly $k(g(q,p))$ distinct values on each level set M_g, i.e.:

$$\{\delta(q,p)|\ (q,p) \in M_g\} = \{\delta_1(g), ..., \delta_{k(g)}(g)\}$$

and $\delta_i(g) \neq \delta_j(g)$ for $i \neq j$. Therefore we may define

$$\delta(l_j^g) = \delta(q,p)|_{(q,p)\in l_j^g} = \delta_j(g)$$

hence

$$S_h(l_j^g) = S_h(q,p)|_{(q,p)\in l_j^g} = (\delta_j(g), g_2, ...g_n).$$

Furthermore, if l_j^g and l_i^g coalesce to a (singular) level set $l_k^{g^*}$ as $g \to g^*$ then $\delta(l_{i,j}^g) \to \delta(l_k^{g^*})$. Summarizing, there is a 1-1 correspondence between the range of S_h and the connected components of the level sets in E_h and this correspondence depends continuously on the phase space points even across singularities. In particular, if the level sets are compact every point at which $S_h(q,p)$ is smooth corresponds to a single n-torus, and every point at which $S_h(q,p)$ is not smooth corresponds to a singular level set.

Figure 9 demonstrates that such a construction is possible for simple systems with singularities of order 1 (namely with $s = 1$).

Definition 3. *The branched surface of an energy surface E_h is given by the surface $S_h(E_h)$, namely it is the $n-1$ dimensional surface embedded in $\mathbb{R}^n$: $\mathcal{F} = \{y|\ y = S_h(q,p), (q,p) \in E_h\}$.*

Definition 4. *Two branched surfaces are equivalent if there exists a diffeomorphism of $\mathbb{R}^n$ which maps one branched surface to the other.*

Corollary 1. *Given an integrable Hamiltonian system, the branched surfaces constructed from two different valid sets of constants of motion (with $H_0 = F_1$) are equivalent.*

In particular, the construction of these surfaces from the EMBD, the frequency space diagram and the constant of motion diagrams are all equivalent, as demonstrated in the previous sections. Nearby energy surfaces correspond usually to a smooth deformations of each other, hence they will usually have equivalent branched

surfaces. For $n = 2$ the branched surfaces are the simplest form of the Fomenko graphs.

7.3. **Topological bifurcations.** When nearby energy surfaces have different topological structure we say they undergo a bifurcation:

Definition 5. *h_c is a topological bifurcation point if the branched surfaces across h_c are not equivalent.*

Changes in the structure of the branched surfaces may occur only if the topology of A_h^S, the singularity manifold for a given energy surface, changes. Below we establish that for $s = 1$ the singularity manifold, A_h^S, changes its structure near folds of the singularity surfaces. Since folds of the singularity surfaces imply extrema and extrema imply resonances the main result follows.

Definition 6. *p_f^c is an $n-k$ $(0 < k < n)$ strongly resonant $n-1$ dimensional singular torus with non degenerate frequency vector if in the suitable Arnold-Liouville-Nekhoroshev coordinates*

$$\frac{dH_0(p_f^c)}{dI_j} = 0, \quad \det\left(\frac{d^2H_0(p_f^c)}{dI_i dI_j}\right) \neq 0, \qquad j = 1, ..., k. \tag{7.3}$$

The relation between equation (7.3) and resonances, as stated in the definition, follows from theorem 1.

Theorem 2. *If p_f^c is a non-parabolic $n-1$ strongly resonant $n-1$ dimensional singular torus with non-degenerate frequency vector then $h_c = H_0(p_f^c)$ is a topological bifurcation point.*

Proof. The theorem essentially follows from Morse lemma (see [24] or [37]); we include some details to enhance the intuition. Using the suitable local Arnold-Liouville-Nekhoroshev coordinates near p_f, we may write

$$H_0(p_f - p_f^c) = H_0(p_f^c) + (I^f - I^c)^T A (I^f - I^c) + O(3) \tag{7.4}$$

where A is the Hessian at p_f^c : $A = \frac{d^2H_0(p_f^c)}{dI_i dI_j}$ (recall that $\nabla_{x,y} H_0(p_f - p_f^c) \equiv 0$). Hence, by linear orthonormal transformation $Uz = I$, we may write eq. (7.4):

$$H_0(p_f - p_f^c) - H_0(p_f^c) + \sum_{i=1}^{n-1-r} a_{i+r} z_{i+r}^2 = \sum_{i=1}^{r} a_i z_i^2 + O(3)$$

where $a_i > 0$, for all i by the non-degeneracy assumption. In fact, r is the Morse index of $h_f(I) = H_0(x_f(I), y_f(I), I)$ at p_f^c (the dimension of the subspace for which the Hessian A is positive definite). The Morse lemma, which applies to $h_f(I)$ by eq. (7.3), states that by smooth local change of coordinates we can eliminate all higher order terms and set all the a_i's to unity. It follows immediately that intersection of the singularity surface $\{H_0(p_f), I_f\}$ with the plane $H_0(p_f) = h$ near p_f^c changes its topology across $h_c = H_0(p_f^c)$; if $r = n-1$ (respectively $r = 0$) namely A is positive (negative) definite, then near p_f^c, for $h < h_c$ $(h > h_c)$ there is no branch of p_f near p_f^c satisfying $H_0(p_f) = h$ whereas on the other side there is an $n-2$ dimensional ellipse satisfying this equation. If $0 < r < n-1$, the hyperboloids $p_f(h, \cdot)$ change their orientation at $h = h_c$, namely, they do not depend smoothly on h at h_c. Since the branched surfaces change across the surfaces $p_f(h, \cdot)$ the claim is proved. □

7.4. **Parabolic tori and topological bifurcations.** Consider the surface of parabolic lower dimensional tori $p_{pf} = (x_{pf}, y_{pf}, I_{pf})$ so that

$$\nabla_{x,y} H_0(x,y,I)\big|_{p_{pf}} = \det \frac{\partial^2 H(x,y,I)}{\partial x \partial y}\bigg|_{p_{pf}} = 0. \tag{7.5}$$

These 3 equations define (generically) a co-dimension two surface in the EMBD, the singularity surface, p^h_{pf}. Along p^h_{pf} two (or more, in symmetric/degenerate cases) singularity surfaces representing families of non-parabolic $(n-1)$-tori, $p^h_{f_i}(I)$, $i = 1,..,n$, meet. For example, in section 6, the four singularity surfaces $p^h_{f_{1,2}}(I) = p^{\pm}_{ell}$, $p^h_{f_{3,4}}(I) = p^0_{hyp,ell}$ meet at $p^h_{pf} = p^0_{par}$. The natural oscillations in the xy plane of the $n-1$ dimensional tori p_{pf} vanish, so these tori are strongly resonant in the ω_0 direction. We now address the natural question in view of theorem 1: when do extremal points of this singularity surface (p^h_{pf}) in the EMBD correspond to additional strong resonances? Here, one should take careful limits when considering derivatives across the singular boundary of $p^h_{f_i}(I)$, namely across p^h_{pf}. To formulate such conditions let us investigate more fully equation (7.5). Define the functions

$$f_1(x,y,I) = \frac{\partial H(x,y,I)}{\partial x},\ f_2(x,y,I) = \frac{\partial H(x,y,I)}{\partial y},\ f_3(x,y,I) = \det \frac{\partial^2 H(x,y,I)}{\partial x \partial y}$$

then equation (7.5) defines the surface $f_1(x,y,I) = f_2(x,y,I) = f_3(x,y,I) = 0$. Can this surface be represented as a graph over the $n-2$ actions $J^{n-2} = (I_1,..,I_{j_p-1}, I_{j_p+1},...,I_{n-1})$ for some chosen index j_p? By the IFT, this may be done if $\frac{\partial(f_1,f_2,f_3)}{\partial(x,y,I_{j_p})}$ is non-singular, hence we define

Definition 7. *p_{pf} is an $n-1$ dimensional parabolic torus which is non-degenerate in the I_{j_p} direction if p_{pf} satisfies (7.5) and*

$$\det \frac{\partial(\frac{\partial H(x,y,I)}{\partial x}, \frac{\partial H(x,y,I)}{\partial y}, \det \frac{\partial^2 H(x,y,I)}{\partial x \partial y})}{\partial(x,y,I_{j_p})}\bigg|_{p_{pf}} \neq 0. \tag{7.6}$$

If p^*_{pf} is an $n-1$ dimensional parabolic torus which is non-degenerate in the I_{j_p} direction then in its neighborhood there is an $n-2$ dimensional family of parabolic tori p_{pf} which may be expressed as a graph over the $n-2$ actions $J^{n-2} = (I_1,..,I_{j_p-1}, I_{j_p+1},...,I_{n-1}) : p_{pf}(J^{n-2}) = (x_{pf}(J^{n-2}), y_{pf}(J^{n-2}), I_{j_p}(J^{n-2}), J^{n-2})$. It follows that the corresponding co-dimension two surface in the EMBD can be represented as a graph over the same actions as well:

$$\begin{aligned} p^h_{pf}(J^{n-2}) &= \{H_0(x_{pf}(J^{n-2}), y_{pf}(J^{n-2}), I_{j_p}(J^{n-2}), J^{n-2}), I_{j_p}(J^{n-2}), J^{n-2}\} \\ &= \{h_{pf}(J^{n-2}), I_{j_p}(J^{n-2}), J^{n-2}\}. \end{aligned}$$

Using eq. (7.5), it follows that:

$$\begin{aligned} \frac{\partial h_{pf}(J^{n-2})}{\partial I_j}\bigg|_{p_{pf}} &= \left(\frac{\partial H(x,y,I)}{\partial I_j} + \frac{\partial H(x,y,I)}{\partial I_{j_p}} \frac{\partial I_{j_p}(J^{n-2})}{\partial I_j}\right)\bigg|_{p_{pf}} \\ &= \left(\dot\theta_j + \dot\theta_{j_p} \frac{\partial I_{j_p}(J^{n-2})}{\partial I_j}\right)\bigg|_{p_{pf}} \quad \text{for } j \neq j_p \end{aligned} \tag{7.7}$$

whereas

$$\dot{\theta}_{j_p}\Big|_{p_{pf}} = \frac{\partial H(x,y,I)}{\partial I_{j_p}}\Big|_{p_{pf}} = \frac{\partial h_{f_i}(I)}{\partial I_{j_p}}\Big|_{p_{f_i}\to p_{pf}} \tag{7.8}$$

and the independence of the last term on i follows from the smooth dependence of the Hamiltonian flow on I, even across the parabolic (in the xy direction) point. The relation between extremal points of $h_{pf}(J^{n-2})$ (at which $\frac{\partial h_{pf}(I)}{\partial I_i}\Big|_{p_{pf}} = 0$) and resonances is now clear:

Theorem 3. *Consider a family of normally parabolic $n-1$ dimensional tori $p_{pf} = (x_{pf}, y_{pf}, I_{pf})$ which is non-degenerate in the I_{j_p} direction at p^c_{pf}. Then, for $j \neq j_p$, extremal point in the I_j direction of the corresponding singularity manifold in the EMBD at p^c_{pf} corresponds to a strong resonance in this direction iff p^c_{pf} is strongly resonant in the I_{j_p} direction or if I_{j_p} is extremal in I_j at p^c_{pf}. p^c_{pf} is strongly resonant in the I_{j_p} direction iff the non-parabolic singularity surfaces emanating from p_{pf} are extremal in the I_{j_p} direction in the limit $p_{f_i} \to p^c_{pf}$.*

Attempt to apply the above theorem to the system (6.1) immediately fails - this system does not satisfy the non-degeneracy condition (7.6). Considering all systems with natural mechanical potential in the xy plane having a parabolic invariant $(n-1)$-torus at the origin:

$$H^{gen}_{bif}(x,y,I) = \frac{y^2}{2} - \frac{x^2}{2}f(I) + V(x,I), \tag{7.9}$$
$$f(0) = 0, \quad \frac{\partial V}{\partial x}\Big|_{(0,0)} = 0, \quad \frac{\partial^2 V}{\partial x^2}\Big|_{(0,0)} = 0,$$

we realize that the non-degeneracy condition (7.6) corresponds to insisting that:

$$\frac{\partial^3 V}{\partial x^3}\frac{\partial^2 V}{\partial x \partial I_{j_p}}\Big|_{(0,0)} \neq 0$$

namely the system is asymmetric w.r.t. reflections in x and the location of the bifurcating invariant tori depends on I_{j_p}.

We observe that another possibility (which is realized in our case of system (6.1)) to satisfy equations (7.5) along a simple $n-2$ dimensional surface is to require that the unperturbed system separates to a sum of two Hamiltonians, the first depending on (x, y, I_{j_p}) and the second depending on the actions $(I_1, ..., I_{n-1})$. In this case equations (7.5) are independent of $J^{n-2} = (I_1, .., I_{j_p-1}, I_{j_p+1}, ..., I_{n-1})$ and any solution of these equations is satisfied for all J^{n-2} values. This separability assumption is of course highly non-generic from mathematical point of view but is certainly of Physical relevance. Define:

Definition 8. *p_{pf} is an $n-1$ dimensional parabolic torus fully degenerate in the I_{j_p} direction, if p_{pf} satisfies (7.5) and these equations are independent of I_j for all $j \neq j_p$.*

This condition is satisfied for any system of the form (7.9) if $f(I) = f(I_{j_p}), V(x,I) = V(x, I_{j_p}) + g(I)$. In this case p_{pf} can be locally presented as the surface $(x_{pf}, y_{pf}, I_{j_p,pf}, J^{n-2})$ with $x_{pf}, y_{pf}, I_{j_p,pf}$ independent of J^{n-2} so $\frac{\partial I_{j_p,pf}}{\partial I_j} = 0$ for $j \neq j_p$. Indeed, for eq. (6.1), we saw that $j_p = 1$ and $p_{pf} = (x_{pf}, y_{pf}, I_{1,pf}, I_2) = (0, 0, 0, I_2)$. Hence, near a parabolic torus, which is fully degenerate in the I_{j_p} direction, we can present the $n-$

2 dimensional family of parabolic tori as: $p^h_{pf}(J^{n-2}) = \{H_0(x_{pf}, y_{pf}, I_{j_p}, J^{n-2}), I_{j_p}, J^{n-2}\} = \{h_{pf}(J^{n-2}), I_{j_p}, J^{n-2}\}$. The relation between extrema of $h_{pf}(J^{n-2})$ and additional resonances follows immediately from equations (7.7) and (7.8), where we use $\frac{\partial I_{j_p}}{\partial I_j} = 0$ to conclude:

Theorem 4. *Consider a family of normally parabolic $n-1$ dimensional tori $p_{pf} = (x_{pf}, y_{pf}, I_{pf})$, which is fully degenerate in the I_{j_p} direction at p^c_{pf}. Then, for $j \neq j_p$, extremal point in the I_j direction of the corresponding singularity manifold in the EMBD at p^c_{pf} corresponds to a strong resonance in this direction. p^c_{pf} is strongly resonant in the I_{j_p} direction iff the non-parabolic singularity surfaces emanating from p_{pf} are extremal in the I_{j_p} direction in the limit $p_{f_i} \to p^c_{pf}$.*

As in section 7.3, by the Morse lemma, $n-2$ non-degenerate folds in the direction of the $n-2$ actions J^{n-2} of the co-dimension two surface $p^h_{pf}(J^{n-2})$ correspond to topological bifurcations. From equations (7.7) and (7.8) we conclude that such folds are not always associated with resonances, and we should distinguish between three cases[9]. For the fully degenerate case folds and resonances are simply related:

Theorem 5. *Consider an $n-1$ dimensional parabolic torus, p^c_{pf}. Assume p^c_{pf} is completely degenerate in the I_{j_p} direction and that p^c_{pf} is $n-2$ strongly resonant with non-degenerate frequency vector in the $I_1, .., I_{j-1}, I_{j+1}, ..., I_{n-1}$ directions, then $h_{pc} = H_0(p^c_{pf})$ is a topological bifurcation point.*

In section 6, the energy $h_{pc} = h^0_p$ is a topological bifurcation point which is well described by this theorem; at h^0_p parabolic tori first appear, and we have seen that a resonance in the I_2 direction occurs there.

In the generic case, a fold of $p^h_{pf}(J^{n-2})$ in the I_j direction is associated with resonance if $\dot{\theta}_{j_p} = 0$ or if $\left.\frac{\partial I_{j_p}(J^{n-2})}{\partial I_j}\right|_{p^c_{pf}} = 0$. Hence, topological bifurcations occurring at an $n-2$ fold of $p^h_{pf}(J^{n-2})$ are associated with a resonance only if additional conditions are satisfied. To satisfy these additional conditions in a persistent way the system must have additional parameters or symmetries:

Theorem 6. *Consider an $n-1$ dimensional parabolic torus, p^c_{pf}. Assume that p^c_{pf} is non-degenerate in the I_{j_p} direction and that the Hamiltonian at p^c_{pf} is locally separable, namely $\left.\frac{\partial I_{j_p}(J^{n-2})}{\partial I_j}\right|_{p^c_{pf}} = 0$ for all $j \neq j_p$. Then, if p^c_{pf} is $n-2$ strongly resonant with non-degenerate frequency vector in the $I_1, .., I_{j-1}, I_{j+1}, ..., I_{n-1}$ directions, then $h_{pc} = H_0(p^c_{pf})$ is a topological bifurcation point. Without imposed symmetries, such a phenomena is of co-dimension $n-2$.*

Theorem 7. *If p^c_{pf} is an $n-1$ dimensional parabolic torus of fixed points which is non-degenerate in the I_{j_p} direction and has non-degenerate frequency vector in the $I_1, .., I_{j-1}, I_{j+1}, ..., I_{n-1}$ direction then $h_{pc} = H_0(p^c_{pf})$ is a topological bifurcation point. Without imposed symmetries, such a phenomena is of co-dimension 1.*

[9]Note that there are two different (independent) types of non-degeneracies - one corresponds to the standard assumption regarding changes in the frequency vector (definition 6) and is needed for applying Morse lemma. The other corresponds to the non-degenerate (degenerate) dependence of the parabolic tori on a specific action (definitions 7,8).

8. Discussion

We have shown that when the Arnold-Liouville-Nekhoroshev coordinates, valid in a neighborhood of a singular level set with $n-1$ dimensional invariant torus, can be extended globally (as in our prototype models of normally stable, unstable and bifurcating tori) the combination of the energy-momentum bifurcation diagram (EMBD) and the branched surfaces supply full qualitative description of the *near-integrable* dynamics: on these diagrams the topological changes in the energy surfaces and the appearance of lower-dimensional resonances are apparent, thus various mechanisms for instabilities (such as homoclinic orbits, hyperbolic resonances and parabolic resonances) may be clearly identified. In particular, we proved that topological bifurcations of the energy surfaces correspond to folds of singularity surfaces in these diagrams and hence to resonances. In other works ([34, 35]) we have demonstrated that the curvature of these singularity surfaces at the folds plays a crucial role in the extent of the instabilities in the perturbed system. Again, such effects are easily identified in these diagrams.

Many issues remain for future studies:

- We have seen (sections 5.3 and 6.3) that there is a long list of instabilities associated with the near-integrable motion near families of lower dimensional tori which is not well understood yet.
- For 2 d.o.f. systems, the description of the energy surfaces as graphs gives a useful insight regarding the evolution of the instabilities in the action variables (or, more generally, in the adiabatic variables of the system) under small conservative perturbations or conservative noise [19]. These ideas were generalized to n d.o.f. systems with strong conservative noise which destroys all integrals of motion and small non-conservative noise which leads to diffusion between different energy surfaces [18]. In view of our work, one is lead naturally to investigation of motion in integrable (or near-integrable) systems with small conservative noise by studying *random motion along branched surfaces*.
- The behavior of systems for which the local Arnold-Liouville-Nekhoroshev coordinates cannot be globally extended is yet to be studied. In particular, one would like to extend the presentation here so it will be applicable to the work of Fomenko and co-workers in which the topology of complicated systems, like the rigid body, are fully analyzed [16, 17]. On one hand, one may use general constants of motion plots in a similar fashion to what we have proposed for the EMBD yet the relation between folds and resonances will be lost. On the other hand, even for such plots, finding the branched surfaces topology from the Fomenko graphs is challenging.
- Finally, the effect of $n-s$ dimensional tori with various stabilities in the $2s$ dimensional normal space for $s>1$ (as in [30]) on the EMBD structure and the branched surfaces structure is yet to be understood.

References

[1] R. Abraham and J. E. Marsden, *Foundations of mechanics*, Benjamin/Cummings Publishing Co. Inc. Advanced Book Program, Reading, Mass., 1978. Second edition, revised and enlarged, With the assistance of Tudor Raţiu and Richard Cushman.

[2] V. I. Arnol'd, *Dynamical Systems III*, vol. 3 of Encyclopedia of Mathematical Sciences, Springer-Verlag, second ed., 1993.

[3] S. V. Bolotin and D. V. Treschev, *Remarks on the definition of hyperbolic tori of hamiltonian systems*, Regul. Chaotic Dyn., 5 (2000), pp. 401–412.
[4] A. V. Bolsinov and A. T. Fomenko, *Trajectory classification of simple integrable hamiltonian systems on three-dimensional surfaces of constant energy*, Dokl. Akad. Nauk (Russian), 332 (1993), pp. 553–555. English trans. in Russian Acad. Sci. Dokl. Math., 48(2), pp 365-369, 1994.
[5] H. W. Broer, G. B. Huitema, and M. B. Sevryuk, *Quasi-periodic tori in families of dynamical systems: order amidst chaos*, vol. 1645 of LNM 1645, Springer Verlag, 1996.
[6] R. Cushman, *The momentum mapping of the harmonic oscillator*, in Symposia Mathematica, Vol. XIV (Convegno di Geometria Simplettica e Fisica Matematica, INDAM, Rome, 1973), Academic Press, London, 1974, pp. 323–342.
[7] R. H. Cushman and L. M. Bates, *Global Aspects of Classical Integrable Systems*, Birkhauser Verlag AG, 1997.
[8] A. Delshams, R. de la Llave, and T. M. Seara, *A geometric approach to the existence of orbits with unbounded energy in generic periodic perturbations by a potential of generic geodesic flows of* $\mathbb{T}^2$, Communications in Mathematical Physics, 209 (2000), pp. 353–392.
[9] H. R. Dullin, M. Juhnke, and P. H. Richter, *Action integrals and energy surfaces of the kovalevskaya top*, Internat. J. Bifur. Chaos Appl. Sci. Engrg., 4 (1994), pp. 1535–1562.
[10] H. R. Dullin, P. H. Richter, and A. P. Veselov, *Action variables of the kovalevskaya top*, Regular and Chaotic Dynamics, 3 (1998), pp. 18–26.
[11] L. H. Eliasson, *Perturbations of stable invariant tori for hamiltonian systems*, Ann. Scuola Norm. Sup. Pisa Cl. Sci. IV, 15 (1988), pp. 115–147.
[12] N. Fenichel, *Persistence and smoothness of invariant manifolds for flows*, Ind. Univ. Math. J., 21 (1971), pp. 193–225.
[13] ———, *Asymptotic stability with rate conditions*, Ind. Univ. Math. J., 23 (1974), pp. 1109–1137.
[14] ———, *Asymptotic stability with rate conditions, II*, Ind. Univ. Math. J., 26 (1977), pp. 81–93.
[15] A. T. Fomenko, *Topological classification of all integrable hamiltonian differential equations of general type with two degrees of freedom*, in The geometry of Hamiltonian systems (Berkeley, CA, 1989), Math. Sci. Res. Inst. Publ., 22, Springer, New York, 1991, pp. 131–339.
[16] A. T. Fomenko, ed., *Topological classification of integrable systems*, vol. 6 of Advances in Soviet Mathematics, American Mathematical Society, Providence, RI, 1991. Translated from the Russian.
[17] ———, *Symplectic topology of integrable dynamical systems. Rough topological classification of classical cases of integrability in the dynamics of a heavy rigid body*, Zap. Nauchn. Sem. S.-Peterburg. Otdel. Mat. Inst. Steklov. (POMI), 235 (1996), pp. 104–183, 305. translation in J. Math. Sci. (New York) 94 (1999), no. 4, 1512–1557.
[18] M. Freidlin and M. Weber, *On random perturbations of Hamiltonian systems with many degrees of freedom*, Stochastic Process. Appl., 94 (2001), pp. 199–239.
[19] M. I. Freidlin and A. D. Wentzell, *Random perturbations of Hamiltonian systems*, Mem. Amer. Math. Soc., 109 (1994).
[20] S. M. Graff, *On the conservation of hyperbolic invariant tori for Hamiltonian systems*, J. Diff. Eq., 15 (1974), pp. 1–69.
[21] J. Guckenheimer and P. Holmes, *Nonlinear Oscillations, Dynamical Systems, and Bifurcations of Vector Fields*, New York: Springer, 1983.
[22] G. Haller, *Chaos Near Resonance*, Applied Mathematical Sciences; 138, Springer-Verlag, NY, 1999.
[23] H. Hanssmann, *The quasi-periodic center-saddle bifurcation*, Journal of Differential Equations, 142 (1997), pp. 305–370.
[24] A. Katok and B. Hasselblatt, *Introduction to the Modern Theory of Dynamical Systems.*, vol. 54 of Encyclopedia of Mathematics and its Applications, Cambridge University Press, 1995.
[25] J. Laskar, *Frequency analysis for multi-dimensional systems. global dynamics and diffusion*, Physica D, 67 (1993), pp. 257–281.
[26] J. Laskar, *Global dynamics and difussion*, Physica D, 67 (1993), pp. 257–281.
[27] L. Lerman and I. Umanskii, *Classification of four dimensional integrable Hamiltonian systems and Poisson actions of* r^2 *in extended neighborhood of simple singular points, i*, Russian Acad. Sci., Sb. Math., 77 (1994), pp. 511–542.

[28] ———, *Classification of four dimensional integrable Hamiltonian systems and Poisson actions of r^2 in extended neighborhood of simple singular points, ii*, Russian Acad. Sci., Sb. Math., 78 (1994), pp. 479–506.

[29] L. M. Lerman and I. L. Umanskii, *Classification of four-dimensional integrable hamiltonian systems and poisson actions of $\mathbb{R}^2$ in extended neighborhoods of simple singular points. III. realizations*, Mat. Sb. (Russian), 186 (1995), pp. 89–102. English trans. in Sb. Math. 186(10), pp 1477-1491, 1995.

[30] L. M. Lerman and Y. L. Umanskiy, *Four-dimensional integrable Hamiltonian systems with simple singular points (topological aspects)*, vol. 176 of Translations of Mathematical Monographs, American Mathematical Society, Providence, RI, 1998. Translated from the Russian manuscript by A. Kononenko and A. Semenovich.

[31] A. Lichtenberg and M. Lieberman, *Regular and Stochastic Motion*, vol. 38 of Applied Mathematical Sciences, Springer-Verlag, 1983.

[32] A. Litvak-Hinenzon, *Parabolic resonances in Hamiltonian systems*, PhD thesis, The Weizmann Institute of Science, Rehovot, Israel, May 2001. Advisor: Prof. V. Rom-Kedar.

[33] A. Litvak-Hinenzon and V. Rom-Kedar, *Parabolic resonances in near integrable hamiltonian systems*, in Stochaos: Stochastic and Chaotic Dynamics in the Lakes, D. S. Broomhead, E. A. Luchinskaya, P. V. E. McClintock, and T. Mullin, eds., American Institute of Physics, Melville, NY, USA, 2000, pp. 358–368. Refereed.

[34] A. Litvak-Hinenzon and V. Rom-Kedar, *Parabolic resonances in 3 degree of freedom near-integrable Hamiltonian systems*, Phys. D, 164 (2002), pp. 213–250.

[35] ———, *Resonant tori and instabilities in Hamiltonian systems*, Nonlinearity, 15 (2002), pp. 1149–1177.

[36] K. R. Meyer and R. G. Hall, *Introduction to Hamiltonian Dynamical Systems and the N-Body Problem*, vol. 90 of Applied Mathematical Sciences, Springer-Verlag, NY, 1991.

[37] J. Milnor, *Morse theory. Based on lecture notes by M. Spivak and R. Wells.*, no. 51 in Annals of Mathematics Studies, Princeton University Press, 1963.

[38] N. N. Nehorošev, *Action-angle variables, and their generalizations*, Trans. Moscow Math. Soc., 26 (1972), pp. 181–198.

[39] A. A. Oshemkov, *Description of isoenergetic surfaces of integrable hamiltonian systems with two degrees of freedom (russian)*, Trudy Sem. Vektor. Tenzor. Anal., 23 (1988), pp. 122–132.

[40] J. Pöschel, *On elliptic lower dimensional tori in Hamiltonian systems*, Math. Z., 202 (1989), pp. 559–608.

[41] V. Rom-Kedar, *Parabolic resonances and instabilities*, Chaos, 7 (1997), pp. 148–158.

[42] V. Rom-Kedar, Y. Dvorkin, and N. Paldor, *Chaotic Hamiltonian dynamics of particle's horizontal motion in the atmosphere*, Physica D, 106 (1997), pp. 389–431.

[43] S. Smale, *Topology and mechanics. I*, Invent. Math., 10 (1970), pp. 305–331.

[44] J. L. Tennyson, M. A. Lieberman, and A. J. Lichtenberg, *Diffusion in near-integrable hamiltonian systems with three degrees of freedom*, in Nonlinear dynamics and the beam-beam interaction (Sympos., Brookhaven Nat. Lab., New York, 1979), vol. 57 of AIP Conf. Proc., Amer. Inst. Physics, New York, 1980, pp. 272–301.

[45] D. Treschev, *Multidimensional symplectic separatrix maps*, J. Nonlinear Sci., 12 (2002), pp. 27–58.

[46] ———, *Trajectories in a neighbourhood of asymptotic surfaces of a priori unstable Hamiltonian systems*, Nonlinearity, 15 (2002), pp. 2033–2052.

[47] H. Waalkens and H. R. Dullin, *Quantum monodromy in prolate ellipsoidal billiards*, Ann. Physics, 295 (2002), pp. 81–112.

Mathematics Institute, University of Warwick, Gibbet Hill Rd., Coventry CV4 7AL, U.K.

E-mail address: litvak@maths.warwick.ac.uk

URL: http://www.maths.warwick.ac.uk/~litvak/

Faculty of mathematical and computer science, Weizmann Institute, Rehovot 76100, Israel

E-mail address: vered@wisdom.weizmann.ac.il

URL: http://www.wisdom.weizmann.ac.il/~vered/